NASA CONTRACTOR REPORT

NASA CR-2725

EQUILIBRIUM CHEMICAL REACTION OF SUPERSONIC HYDROGEN-AIR JETS (THE ALMA COMPUTER PROGRAM)

S. Elghobashi and D. B. Spalding

Prepared by
FLUID MECHANICS & THERMAL SYSTEMS, INC.
Waverly, Ala. 36879
for Langley Research Center

NATIONAL AERONAUTICS AND SPACE ADMINISTRATION • WASHINGTON, D. C. • JANUARY 1977

1. Report No.	2. Government Accession No.	3. Recipient's Catalog No.
NASA CR-2725		

4. Title and Subtitle	5. Report Date
EQUILIBRIUM CHEMICAL REACTION OF SUPERSONIC HYDROGEN-AIR JETS (THE ALMA COMPUTER PROGRAM)	January 1977
	6. Performing Organization Code
7. Author(s)	8. Performing Organization Report No.
S. Elghobashi and D. B. Spalding	
9. Performing Organization Name and Address	10. Work Unit No.
Concentration, Heat and Momentum Limited 86 Burlington Road, New Malden, England Subcontractor to: Fluid Mechanics & Thermal Systems, Inc. Route 2, Box 11, Waverly, AL 36879	505-05-41-02
	11. Contract or Grant No. NAS1-13729
12. Sponsoring Agency Name and Address	13. Type of Report and Period Covered
National Aeronautics & Space Administration Washington, DC 20546	Contractor Report
	14. Sponsoring Agency Code

15. Supplementary Notes

Langley technical monitor: John S. Evans, Jr.

Final report.

16. Abstract

The ALMA (Axi-symmetrical Lateral Momentum Analyser) program is concerned with the computation of 2-dimensional coaxial jets with large lateral pressure gradients. The jets may be free or confined, laminar or turbulent, reacting or non-reacting. Reaction chemistry is equilibrium.

17. Key Words (Suggested by Author(s))	18. Distribution Statement
Pressure gradient Coaxial jet Turbulent mixing Hydrogen-air Combustion	Unclassified - Unlimited Subject Category 34

19. Security Classif. (of this report)	20. Security Classif. (of this page)	21. No. of Pages	22. Price*
Unclassified	Unclassified	57	$4.25

* For sale by the National Technical Information Service, Springfield, Virginia 22161

CONTENTS

LIST OF FIGURES

LIST OF FIGURES (Continued)

LIST OF FIGURES (Continued)

LIST OF TABLES

LIST OF SYMBOLS AND ACRONYMS

a	used to denote the power to which weighting function raised
A	effective cloud amount ($A=N\varepsilon$)
A_L	effective cloud amount for the lower of two layers
A_u	effective cloud amount for the upper of two layers
A*	a function of A_L and A_u
A_{Total}	sum of effective cloud layers
B	Planck function (radiance)
B_r	Planck radiance at frequency r
CO_2	carbon dioxide
C	a numerical correction
$\hat{C}$	a computed estimate of C
c_1, c_2	constants used in computing temperature
G	the quantitative difference between the average radiances arising from the clear and cloudy portions of a field of view (FOV)
H_2O	water vapor
I	clear column radiance
$\tilde{I}$	measured radiance for a cloudless atmosphere
$\tilde{I}$*	measured cloud-contaminated radiance
I*	a computed estimate of $\tilde{I}$*
I_{MEAS}	measured radiance
I_{CD}	average radiance arising from the cloudy portion of the FOV
I_{CLR}	average radiance arising from the clear portion of the FOV (equivlanet clear column radiance when obtained by filtering cloud effects)
$\bar{I}$	clear column radiance averaged over many FOVs

1. INTRODUCTION

1.1 The ALMA code

The ALMA (Axi-symmetrical Lateral Momentum Analyser) computer program is concerned with the numerical computation of two-dimensional coaxial jets with large lateral pressure gradients. The jets may be free or confined, laminar or turbulent, reacting or non-reacting.

In its present version, ALMA predicts the mass fractions of the products of combustion of hydrogen and oxygen, based on the assumption of chemical equilibrium.

1.2 Connections with previous work

Under a previous contract (NAS1-12167), a computer code, CHARNAL, was developed for predicting the mixing and combustion of turbulent coaxial hydrogen-air jets. CHARNAL was based on the assumption that the pressure of the gases varied with axial distance only; lateral pressure gradients were regarded as negligible. ALMA accounts for these lateral pressure gradients.

The common features between ALMA and CHARNAL are:

- Both codes account for the effects of temperature and composition on local fluid properties such as laminar viscosity and specific heat of the gas mixture.
- Both codes allow for incorporating any inlet-flow conditions (temperature and velocity etc.).
- Both codes have provision for printing some or all of the dependent variables at pre specified axial distances, or after a certain number of marching steps.

1.3 Layout of the report

The remainder of this report is divided into four sections. Section 2 is concerned with the mathematical formulation and physical models employed in ALMA. Section 3 outlines the

SIMPLE algorithm used to link the lateral momentum equation with both the continuity and streamwise momentum equations. In Section 4, sample predictions for some test cases specified by NASA Langley are discussed. Suggestions for further extensions and refinements of ALMA are included in Section 5. Appendix C details the input quantities required for using ALMA.

2. THE MATHEMATICAL AND PHYSICAL ANALYSIS

2.1 Introduction

This chapter details the mathematical and physical basis of the ALMA code. Section 2.2 is concerned with the conservation equations of momentum, stagnation enthalpy and chemical species. Section 2.3 describes the turbulence model; and in Section 2.4 the chemical-equilibrium combustion model is discussed.

2.2 The mean-flow conservation equations

The differential equations listed in this section are the ones which express the conservation of momentum, mass, energy and chemical species in a two-dimensional, axi-symmetric, boundary-layer* flow with large gradients of lateral pressure.

The streamwise momentum equation:

$$\rho u \frac{\partial u}{\partial x} + \rho v \frac{\partial u}{\partial r} = - \frac{\partial p}{\partial x} + \frac{1}{r} \frac{\partial}{\partial r} (\mu_t r \frac{\partial u}{\partial r}) \qquad (1)$$

The lateral momentum equation: (viscous terms being neglected)

$$\rho u \frac{\partial v}{\partial x} + \rho v \frac{\partial v}{\partial r} = - \frac{\partial p}{\partial r} \qquad (2)$$

---

* "Boundary-layer", in this context, refers to the characteristic absence of influences from downstream on upstream events.

The continuity equation:

$$\frac{\partial}{\partial x}(\rho u) + \frac{1}{r}\frac{\partial}{\partial r}(\rho v r) = 0 \qquad (3)$$

Conservation equation of the mixture fraction (≡ the mass fraction of hydrogen in any form) (f):

$$\rho u \frac{\partial f}{\partial x} + \rho v \frac{\partial f}{\partial r} = \frac{1}{r}\frac{\partial}{\partial r}\left(\Gamma_f r \frac{\partial f}{\partial r}\right) \qquad (4)$$

Conservation of stagnation enthalpy ($\tilde{h}$):

$$\begin{aligned}\rho u \frac{\partial \tilde{h}}{\partial x} + \rho v \frac{\partial \tilde{h}}{\partial r} = {} & \frac{1}{r}\frac{\partial}{\partial r}\left(\Gamma_{\tilde{h}} r \frac{\partial \tilde{h}}{\partial r}\right) \\ & + \frac{1}{r}\frac{\partial}{\partial r}\left\{r\mu_t \left(1 - \frac{1}{\sigma_{\tilde{h}}}\right) u \frac{\partial u}{\partial r}\right\} \\ & + \frac{1}{r}\frac{\partial}{\partial r}\left\{r\mu_t \left(\frac{1}{\sigma_k} - \frac{1}{\sigma_{\tilde{h}}}\right) \frac{\partial k}{\partial r}\right\} \\ & + \frac{1}{r}\frac{\partial}{\partial r}\left\{r\mu_t \sum_j \left(\frac{1}{\sigma_{m_j}} - \frac{1}{\sigma_{\tilde{h}}}\right) h_j \frac{\partial m_j}{\partial r}\right\} \qquad (5)\end{aligned}$$

The temperature of the mixture, T, is obtained from known values of $\tilde{h}$, v, u and the mass fractions of the chemical constituents of the mixture as follows:

$$\tilde{h} - \frac{u^2+v^2}{2} - k = h = \sum_j m_j h_j \qquad (6)$$

The species enthalpy, h_j, is defined as :

$$h_j \equiv \int_{T_{ref}}^{T} c_{p,j}\, dT + H_{j,T_{ref}} \qquad (7)$$

where T_{ref} is the temperature of the state from which enthalpy is measured, is usually taken as 298.15 K, and $H_{j,T_{ref}}$ denotes the heat of formation of the species j at T_{ref}. Equation (2.2-7) can then be written as

$$h_j = \int_{298.15\ K}^{T} c_{p,j}\, dT + H_{j,298.15\ K} \qquad (8)$$

$$= \int_{0\ K}^{T} c_{p,j}\, dT + \{H_{j,298.15\ K} - (h_{298.15\ K} - h_{0\ K})\}$$

$$= \overline{c_{p,j}}\, T + H_o \qquad (9)$$

here $\overline{c_{p,j}}$, defined as $\frac{1}{T}\int_{0\ K}^{T} c_{p,j}dT$, denotes a mean specific heat, and H_o is defined by:

$$H_o \equiv H_{j,298.15\ K} - (h_{298.15\ K} - h_{0\ K}) \qquad (10)$$

2.3 The turbulence model

2.3.1 The turbulent viscosity

The effective turbulent-transport coefficients μ_t, Γ_h, Γ_f are determined by means of the k-ε model of turbulence (ref. 1). According to this model, the magnitude of the viscosity depends only on the local values of the turbulence kinetic energy, k, on the dissipation rate of turbulence energy, ε, and on the fluid density. This turbulent viscosity μ_t, is given by:

$$\mu_t = C_\mu\, \rho\, k^2/\varepsilon \qquad (11)$$

where C_μ is a constant.

The quantities k and ε are computed for each point in the field by way of the following pair of transport equations:

$$\rho u \frac{\partial k}{\partial x} + \rho v \frac{\partial k}{\partial r} = \frac{1}{r} \frac{\partial}{\partial r} \left(\frac{\mu_t}{\sigma_k} r \frac{\partial k}{\partial r}\right) + \mu_t \left(\frac{\partial u}{\partial r}\right)^2 - \rho\varepsilon, \qquad (12)$$

$$\rho u \frac{\partial \varepsilon}{\partial x} + \rho v \frac{\partial \varepsilon}{\partial r} = \frac{1}{r} \frac{\partial}{\partial r} \left(\frac{\mu_t}{\sigma_\varepsilon} r \frac{\partial \varepsilon}{\partial r}\right) + C_1 \frac{\varepsilon}{k} \mu_t \left(\frac{\partial u}{\partial r}\right)^2 - C_2 \frac{\rho\varepsilon^2}{k} \qquad (13)$$

2.3.2 The concentration fluctuations

Another important turbulence quantity is the time-mean square of the fluctuations of mixture fraction g. This quantity can be used to account for the effect of turbulence on the rate of chemical reaction (Ref. 2) or to estimate the width of a turbulent-flame brush (Ref.3). In ALMA, this width, which is defined as the region of flow over which the stoichiometric conditions occur, is calculated as follows.

First, the magnitude of the mean-square fluctuations of the mixture fraction, g, is found from the solution of the following transport equation developed by Spalding (Ref.4):

$$\rho u \frac{\partial g}{\partial x} + \rho v \frac{\partial g}{\partial r} = \frac{1}{r} \frac{\partial}{\partial r} \left(\frac{\mu_t}{\sigma_g} r \frac{\partial g}{\partial r}\right) + C_{g1} \mu_t \left(\frac{\partial f}{\partial r}\right)^2 - C_{g2} \frac{\rho\varepsilon g}{k} \qquad (14)$$

In the above equation, the values of the constants σ_g, C_{g1} and C_{g2} are 0.7, 2.8 and 2 respectively.

Secondly, a battlement-shaped distribution of the mixture fraction vs time is assumed (Ref. 3); this means that the instantaneous mixture fraction fluctuates rapidly between an upper and lower value, and spends no time in between. From this distribution, and from the values of f and g, the upper and lower values, f_+ and f_-, of the instantaneous mixture fraction are calculated.

Finally, the width of the turbulent flame brush at any downstream location is obtained by determining the two radii at which f_+ and f_- equal f_{st}.

2.4 The combustion model

2.4.1 Equations

Reference (5) describes an equilibrium-chemistry model, developed and used in conjunction with the CHARNAL computer program to predict the properties in a hydrogen-oxygen flame. The main features of the model are described below.

Four equilibrium reactions are assumed as follows:

$$O + O \rightarrow O_2 \qquad (15)$$

$$H + H \rightarrow H_2 \qquad (16)$$

$$H + OH \rightarrow H_2O \qquad (17)$$

$$O + H \rightarrow OH \qquad (18)$$

The six species involved in these reactions are considered to be present in the mixture, together with nitrogen, which is inert. To assist in developing the equations to predict the equilibrium concentration of the species, two intermediate quantities are defined, namely:

$$f \equiv m_{H_2} + m_H + \frac{W_{H_2}}{W_{H_2O}} m_{H_2O} + \frac{W_H}{W_{OH}} m_{OH} \qquad (19)$$

and

$$F \equiv m_{O_2} + m_O + \frac{W_O}{W_{OH}} m_{OH} + \frac{W_O}{W_{H_2O}} m_{H_2O} \qquad (20)$$

where f is the total mass fraction of hydrogen in any form, and F is the total mass fraction of oxygen in any form.

Also required is the auxiliary relation which states that the sum of the mass fractions of all elemental species must be unity:

$$f + F + m_{N_2} = 1 \tag{21}$$

One assumption is now introduced: it is presumed that the coefficients of turbulent diffusion of the chemical species are equal to each other at every point in the flow. A well-known consequence is that f is linearly related to m_{N_2}; and the constants in the relation can be determined from the boundary conditions:

$$\frac{m_{N_2}}{m_{N_2,air}} = 1 - f \tag{22}$$

What remains now is to define the necessary equilibrium constants.

As is common in thermodynamics, the equilibrium constant, K_p, is defined for the reaction aA + bB ——> cC by:

$$K_p \equiv \frac{X_C^c}{X_A^a \, X_B^b} \, p^{c-a-b} \tag{23}$$

where p is the pressure in atmospheres and X_j is the mole fraction of species j. For each of the four reactions in the present model, (c-a-b) equals -1.

It is convenient to express the concentrations in terms of mass fractions using the relation:

$$m_j = \frac{W_j}{W} X_j \tag{24}$$

Substitution of equation (24) into (23) permits derivation of the modified equilibrium constant K_p', thus:

$$K_p' = K_p \; p \; W \frac{W_C^c}{W_A^a \; W_B^b} = \frac{m_C^c}{m_A^a \; m_B^b} \tag{25}$$

The modified equilibrium constants for the reactions (15), (16), (17) and (18) can then be written as:

$$K_1' = \frac{m_{H_2}}{m_H^2} \tag{26}$$

$$K_2' = \frac{m_{O_2}}{m_O^2} \tag{27}$$

$$K_3' = \frac{m_{H_2O}}{m_H \; m_{OH}} \tag{28}$$

and

$$K_4' = \frac{m_{OH}}{m_O \; m_H} \tag{29}$$

If thermodynamic equilibrium prevails, the K'-s take values which depend upon temperature alone. Their values are given in Appendix B.

In the above set of equations, there are 7 unknowns (m_{H_2}, m_{O_2}, m_O, m_{OH}, m_{H_2O}, m_{N_2} and F; f being given) and

7 equations { (19), (20), (21), (26), (27), (28) and (29)} .

The problem is therefore soluble.

2.4.2 Solution procedure

The solution procedure is an iterative one, operating on the two equations:

$$\sqrt{m_{O_2}} = \frac{F}{\left[\frac{\bar{B} + \frac{8}{9}\bar{C}\,m_{H_2} + \frac{16}{17}\bar{D}\sqrt{m_{H_2}}}{2}\right] + \sqrt{\left\{\frac{\bar{B} + \frac{8}{9}\bar{C}\,m_{H_2} + \frac{16}{17}\bar{D}\sqrt{m_{H_2}}}{2}\right\}^2 + F}} \qquad (30)$$

$$\sqrt{m_{H_2}} = \frac{f}{\left[\frac{\bar{A} + \frac{1}{17}\bar{D}\sqrt{m_{O_2}}}{2}\right] + \sqrt{\left\{\frac{\bar{A} + \frac{1}{17}\bar{D}\sqrt{m_{O_2}}}{2}\right\}^2 + \left\{1 + \frac{1}{9}\bar{C}\sqrt{m_{O_2}}\right\} f}} \qquad (31)$$

Here the quantities $\bar{A}.\bar{B},\bar{C},\bar{D}$ are defined by:

$$\bar{A} = \frac{1}{\sqrt{K_1'}} \qquad (32)$$

$$\bar{B} = \frac{1}{\sqrt{K_2'}} \qquad (33)$$

$$\bar{C} = \frac{K_3' K_4'}{K_1'\sqrt{K_2'}} \qquad (34)$$

and

$$\bar{D} = \frac{K_3'}{\sqrt{K_1' K_2'}} \qquad (35)$$

These quantities depend upon temperature alone, and can be tabulated at the start.

Equations (30) and (31) have been derived from equations (19), (20), (21), (26), (27), (28) and (29) by straightforward algebraic manipulation, including the use of the formula for the roots of a quadratic equation.

Because the RHS of equations (30) and (31) contains m_{O_2} and m_{H_2} as well as f and F, iteration is necessary. Direct substitution of the latest guesses for m_{H_2} and m_{O_2} is employed in ALMA, and has been found to be satisfactory in the circumstances which have been investigated; but a Newton-Raphson technique could be employed if divergence were encountered.

3. THE NUMERICAL SOLUTION PROCEDURE

3.1 Introduction

The numerical procedure, employed here to solve the set of partial differential equations that govern the flow and combustion of axi-symmetric boundary layers, is of the marching-integration type. Because of the need in supersonic flows to solve the lateral momentum equation (2) simultaneously with the other conservation equations, a new algorithm (SIMPLE = Semi Implicit Pressure Linked Equations) is introduced to link the streamwise and radial momentum equations with the continuity equation, so as to obtain a pressure field. The remainder of this chapter outlines the basic features of this algorithm and of the numerical procedure.

3.2 The finite-difference grid

Figure 1 shows a portion of the finite-difference grid on the x-r and the x-ω coordinates, where ω is a dimensionless stream function (Ref.6).

The variables u(the x-wise velocity component), p(the pressure), and ρ(the denisty) are all defined at the grid nodes. The lateral velocity component, v, is defined at locations (o's) midway between those of the u-velocity, as shown in Figure 1, in conformity with usual "staggered-grid" practices. The definition entails that the pressures, of which the differences affect v, straddle the v location.

3.3 The formulation of the solution algorithm

Three main steps are followed here to formulate the solution algorithm. The first step is to use the Patankar-Spalding (Ref. 6) procedure to obtain a formula which connects the value of a dependent variable at a downstream node with its value at an upstream node. The second is to use the lateral momentum equation to derive a formula which relates the radial velocity component at a node $(i + \frac{1}{2})$ to the pressures at the nodes (i + 1 and i) which straddle the v-node at the same axial location. The third step is to derive a"pressure correction" equation and use it to determine a pressure field which satisfies both the streamwise and lateral momentum equations and the continuity equation.

Each of the above three steps is discussed below.

3.3.1 The Patankar-Spalding procedure

This procedure is detailed in Reference 6, therefore only the main features are discussed here.

(i) The primary differential equations (1),(4),(5),(12), (13) and (14) are transformed so that the independent variables are the longitudinal distance x and the dimensionless stream function ω defined as:

$$\omega \equiv (\Psi - \Psi_I)/(\Psi_E - \Psi_I) \tag{36}$$

where Ψ is obtained from

$$\frac{\partial \Psi}{\partial r} = \rho u r$$

Subscripts I and E refer respectively to the "inner" and "outer" boundaries of the flow. The resulting differential equations are all of the form:

$$\frac{\partial \phi}{\partial x} + (a + b\omega)\frac{\partial \phi}{\partial \omega} = \frac{\partial}{\partial \omega}\left(c \frac{\partial \phi}{\partial \omega}\right) + d \tag{37}$$

where the terms on the left-hand side represent convection and those on the right hand side express the diffusion and source of the variable ϕ. The coefficients a and b are functions of the entrainment rates, whilst c involves the effective diffusion coefficient.

(ii) The differential equations are expressed as finite-difference equations, connecting the values of ϕ at the nodes i, i + 1, i - 1 (Figure 1) at a downstream station D with those at the corresponding nodes at the upstream station U. The general form of the finite-difference equation is:

$$D_i \phi_{i,D} = A_i \phi_{i+1,D} + B_i \phi_{i-1,D} + E_i \phi_{i,U} + G_i \phi_{i+1,U} + H_i \phi_{i-1,U} + S_i \qquad (38)$$

where A_i, B_i, etc., are treated as constants, the expressions for which are deduced by integration of the differential equation (37) over a control volume surrounding the node where ϕ_i prevails.

(iii) The integration proceeds by "marching" downstream, the values of ϕ_i at station D being calculated from those at station U.

At each forward step, new values are ascribed to Ψ_E and Ψ_I, the stream functions at the grid boundaries. These values, together with the continuity equation, determine the geometrical locations of the boundaries.

3.3.2 The relation between v and p

The relation between v and p is obtained by integrating the lateral momentum equation (2). The finite-difference form of this relation is:

$$v_{i+\frac{1}{2},D} - v_{i+\frac{1}{2},U} = \left[\frac{\delta x}{\rho u}\right]_{i+\frac{1}{2},D} \left[\frac{p_i - p_{i+1}}{r_{i+1} - r_i}\right]_D \qquad (39)$$

where the notations of Figure 1 are used.

Equation (39) shows that a solution for $v_{i+\frac{1}{2},D}$ cannot be obtained in an explicit manner since the radial pressure distribution at D is not a pre-specified quantity. This problem is dealt with in the following section.

3.3.3 The pressure correction procedure (SIMPLE)

The central idea of the pressure-correction procedure is to make an informed guess of the pressure distribution at the downstream station D; then corrections are added to the pressures, and to the velocity components u, v, to ensure compatibility of flow areas.

In this section it is aimed to derive a pressure-correction equation of the form:

$$-c_{i+\frac{1}{2}}\, p'_{i+1} - c_{i-\frac{1}{2}}\, p'_{i-1} + \left\{ c_{i+\frac{1}{2}} + c_{i-\frac{1}{2}} + \frac{A_i^*}{\gamma p_i^*} - \frac{A_i^*}{\rho_i^*\, u_i^{*2}} \right\} p'_i = A_i^* - a_i^* \qquad (40)$$

where the superscripts (*) and (′) denote respectively a guessed quantity and a correction component. In equation (40) the right-hand side is the area-discrepancy appropriate to the guessed velocity field; A^* being the flow area associated with the continuity and streamwise momentum equations and a^* being the area associated with the lateral momentum equation. The c's are coefficients having the dimensions of area divided by pressure.

It is important to note that the solution of the pressure-correction equation (40) yields a pressure-correction component which, when added to the guessed pressure, cancels the discrepancy in the flow areas.

Equation (40) will now be derived.

Three steps are followed in the derivation. The first is to obtain a $p' \sim a'$ relation; the second is to find a $p' \sim A'$ relation, and the third is to combine those two relations to produce equation (40).

p'~a' relation

It is sought to obtain an equation in the form:

$$a'_i = c_{i+\frac{1}{2}} (p'_i - p'_{i+1}) + c_{i-\frac{1}{2}} (p'_i - p'_{i-1}) \qquad (41)$$

where c's are coefficients having the dimensions of area divided by pressure. The starting equation is that which links v and p, i.e. equation (39).

Let the downstream quantities u,v,p,ρ,A,a,r be composed of two components according to:

$$p = p^* + p' \qquad (42)$$
$$u = u^* + u' \qquad (43)$$
$$v = v^* + v' \qquad (44)$$
$$\rho = \rho^* + \rho' \qquad (45)$$
$$A = A^* + A' \qquad (46)$$
$$a = a^* + a' \qquad (47)$$
$$r = r^* + r' \qquad (48)$$

Substitution into equation (39) of the values of p,u,v,ρ,r from equations (42), (43), (44), (45) and (48), followed by subtraction of the resulting equation from (39) yields:

$$v'_{i+\frac{1}{2}} = \left(\frac{\delta x}{\rho^* u^*}\right)_{i+\frac{1}{2}} \left\{\frac{p'_i - p'_{i+1}}{r^*_{i+1} - r^*_i}\right\} \qquad (49)$$

where ρ, u and r are approximated by their guessed values.

Another equation is required to connect a' with v'; this is obtained by referring to Figure 1. The cross-stream area a_i, at D, for the shaded control volume associated with node i can be calculated from:

$$a_i = a_{i,U} + \left\{ r_{i+\frac{1}{2},U} \tan \alpha_{i+\frac{1}{2}} - r_{i-\frac{1}{2},U} \tan \alpha_{i-\frac{1}{2}} \right\} \delta x \qquad (50)$$

where $a_{i,U}$ is the upstream cross-stream area. The inclination α of the constant-ω lines is given by:

$$\alpha = \frac{v}{u} - \frac{\dot{m}'''}{\rho u} \qquad (51)$$

where $\dot{m}'''$ is the rate of mass flow across the constant-ω line.

Substitution into equation (50) of the values of α, r, v, u, v' from equations (51),(48),(44),(43) and (49), followed by subtraction of the resulting equation from equation (50), leads to the desired equation (41), where c now has the value $r\,\delta^2 x/(\delta r\, \rho^*\, u^{*2})$.

<u>$p' \sim A'$ relation</u>

The desired $p' \sim A'$ equation is

$$A_i' = - \left\{ \frac{1}{\gamma p_i^*} - \frac{1}{\rho_i^*\, u_i^{*2}} \right\} A_i^*\, p_i' \qquad (52)$$

which expresses the effect of pressure change on the downstream cross-stream area. Three equations are employed to derive equation (52). These are the continuity, the streamwise momentum equations and the gas-law relation for isentropic expansion.

The mass flow rate across the downstream face of the shaded control volume (Figure 1) is:

$$\rho_i \, u_i \, A_i = (\Psi_E - \Psi_I)(\omega_{i+\frac{1}{2}} - \omega_{i-\frac{1}{2}})$$

$$= \rho_i^* \, u_i^* \, A_i^* \qquad (53)$$

Substitution into equation (53) of the values of ρ, u, A from equations (45), (43), (46) gives:

$$\frac{\rho_i'}{\rho_i^*} + \frac{U_i'}{U_i^*} + \frac{A_i'}{A_i^*} = 0 \qquad (54)$$

where the terms containing the cross products $\rho' u'$, $\rho' A'$, $u' A'$, $\rho' u' A'$ have been neglected.

Now the variation of u with pressure can be estimated by noting that, if the shear stresses and body forces are supposed to be uninfluenced by the pressure change, the streamwise momentum equation (1) leads to:

$$\frac{du}{dp} = - \frac{1}{\rho u} \qquad (55)$$

The substitution of equations (42), (43), (45) into (55) yields:

$$u_i' = - \frac{1}{\rho_i^* \, u_i^*} \, p_i' \qquad (56)$$

Further if the process of pressure adjustment is assumed to be isentropic, then:

$$\rho_i' = \frac{\rho_i^*}{\gamma p_i^*} \, p_i' \qquad (57)$$

Now the $p' \sim A'$ equation (52) can be easily deduced by combining equations (54), (56) and (57).

Finally the pressure-correction equation (40) can now be obtained by noting that the net effect of the pressure-correction process is to cancel the discrepancy in the calculated cross-stream flow areas, i.e. A_i should be equal to a_i or

$$A_i^* + A_i' = a_i^* + a_i' \tag{58}$$

The direct substitution of equations (41), (52) into (58) produces the pressure-correction equation (40) for the node i; similar equations are obtained for all the nodes across the grid.

3.4 Conditions at the E-boundary in supersonic flow

When the free stream is supersonic, the values of u and v at the E-boundary are evaluated from the following two equations:

$$\left[u_2 - u_1\right]_E = (p_2 - p_1)/(\rho_1 u_1) \tag{59}$$

$$\text{and } \left[v_2 - v_1\right]_E = \frac{p_2-p_1}{\rho_1 u_1}\left\{\frac{1}{\tan\left[\alpha_1+\sin^{-1}\left(\frac{c_1}{\sqrt{u_1^2+v_1^2}}\right)\right] - \tan\alpha_1}\right\} \tag{60}$$

where the notations of Figure 2 are used, and c_1 is the speed of sound at station 1.

Equation (59) is derived from the one-dimensional streamwise momentum equation for the shaded control volume (Figure 2). Equation (60) is obtained by combining the equations of continuity and lateral momentum for the shaded control volume and then substituting for the angle $(\theta - \alpha_1)$ between the streamline and the shock from small-wave theory.†

It is seen from equation (60) that the velocity v_2 at the E-boundary can be calculated in terms of quantities immediately upstream. The pressure p_2 at the E-boundary is set equal to the value calculated at the near-boundary node.

3.5 The basic solution steps

The solution procedure will now be reviewed, based on a consideration of the portion of the finite-difference grid shown in Figure 1. The variables at station D are to be determined by the integration of the governing differential equations over the shaded control volume. This integration is performed as follows:

a) The pressure gradient across the forward step is guessed; the pressure p^* at station D is then calculated.

b) Equation (1) is integrated as in Ref. (6). The resulting velocities at D are only estimates since they result from a guessed pressure field.

---

† From small-wave theory, the angle $(\theta - \alpha_1)$ is given by:

$$\theta - \alpha_1 = \sin^{-1}\left[\frac{c_1}{\sqrt{u_1^2+v_1^2}}\right]$$

where c_1 is the speed of sound at station 1.

c) The continuity equation (3) is integrated to yield the radial locations (r_i) of the constant ω lines at D. The area A_i of the downstream face of the control volume (shown shaded in Figure 1) is deduced therefrom.

d) The lateral momentum equation (2) is integrated to yield the v^* velocities at D; these velocities are only estimates, since the pressure field is a guessed one.

e) The inclinations (α_i) of the constant-ω lines are calculated from the values of the v velocities at D. Now it is possible to re-evaluate the area of the downstream face of the control volume from the knowledge of α_i. The new area value is denoted a_i.

f) The values of A_i and a_i would be identical if the guessed values of the pressure field were the correct ones. In practice, however, there is a discrepancy between A_i and a_i; for the former was calculated from the streamwise momentum and the continuity equations, whereas the latter was calculated from the lateral momentum equation.

g) In order to eliminate the discrepancy between the values of a_i and A_i, a pressure-correction component is introduced into the analysis with the net effect of yielding a correct pressure field that will satisfy simultaneously the equations of: streamwise momentum, lateral momentum and continuity and hence cancels the imbalance in the values of a_i and A_i. The pressure corrections are obtained from solving the set of equations such as (40) by the tri-diagonal matrix algorithm.

h) The guessed pressure field and the associated velocity fields are then augmented by the calculated correction

components; the result is a more correct flow field, which certainly satisfies continuity, and which satisfies momentum as accurately as is desired .

i) The above operations (a to h) complete one integration step; they are to be repeated for successive forward steps until the whole domain of integration has been covered.

4. DISCUSSION OF SAMPLE PREDICTIONS

To demonstrate the general capabilities of ALMA, five test cases have been computed; these involve the mixing and combustion of two coaxial jets of hydrogen and air. The geometry and the initial conditions for the test cases are given in Figure 3 and Table 1.

In this section, the results are presented in the form of radial profiles of the quantities u,v,T,k,ε,f,g,ℓ and of the mass fractions of the species O_2, H_2, H_2O, H, O, OH and N_2 in Figures 4 to 17 inclusive. Because the values of the above quantities vary by orders of magnitude and are plotted, at a given station, for convenience in two figures, each is normalized by reference to its maximum and minimum values in the profile, so that the normalized values extend from 0 to 1.

4.1 The jet surrounding a centre-body

Case 1. The results are discussed by examining the radial distributions of the quantities u,v,T,k,ε,f,g and ℓ and the mass fractions of species at three different downstream stations: x/Y_j = 20, 60 and 100 (Figures 4,6,8,5,7 and 9).

Profiles at x/Y_j = 20

Figure 4 shows that at x/Y_j = 20 (i.e. nearest to the nozzle) all the predicted quantities behave as expected. For example, the u-profile exhibits a steep gradient near the

Table 1. Initial Conditions of the Test Cases

Test Case	1	2	3	4	5
p_I $(10^5 N/m^2)$	1.	1.	1.	2.	1.
p_E $(10^5 N/m^2)$	1.	1.	1.	1.	1.
T_I (K)	316.	180.	247.	247.	247.
T_E (K)	885.	885.	1459.	1459.	1459.
T_w (K)	300.	300.	-	-	900.
U_I (m/s)	1303.	2100.	2389.	2389.	2389.
U_E (m/s)	1800.	1800.	1432.	1432.	1432.
Y_j (m)	0.00264	0.00264	-	-	-
R_j (m)	-	-	0.00238	0.00238	0.00238
R_w (m)	0.01214	0.01214	-	-	0.01633
m_{O_2}) outer	.232	.232	.232	.232	.232
m_{N_2}) jet	.768	.768	.768	.768	.768
m_{H_2}) inner jet	1.	1.	1.	1.	1.

centre-body wall and a less steep one in the shear layer between the jet and the free stream.

Also, as is well known, the k-profile (Figure 4) attains a maximum at about the middle of the shear layer where both u and v have large gradients. The dissipation rate of turbulence energy is highest near the wall, where the length scale of turbulence is at its minimum.

Chemical reaction is evident by the peak in the temperature profile (Figure 4) at the radial location where the mixture fraction, f, attains its stochiometric value, f_{st}, of about 0.028.

The mean square of f-fluctuations, g, reaches its maximum value where f has its steepest radial gradient; this is as expected.

Figure 5 shows that the radicles O and OH have their maximum concentrations at the peak temperature, whereas H attains its highest value at a slightly lower temperature towards the hydrogen-rich region.

It is also displayed in Figure 5 that the profiles of H_2 and O_2 overlap in a small region centered around the location of f_{st}. The two species N_2 and H_2O exist in considerable concentration over the whole domain, thought their peaks lie in the air-rich and the hydrogen-rich regions respectively.

Profiles at $x/Y_j = 60$

Figure 6 shows that at a distance 60 Y_j downstream, the shear flow develops and the initial step-shaped u-profile becomes relatively smooth. The maximum values of k and ε are consequently lower than those at the upstream station of 20 Y_j.

The temperature profile still has its maximum near the location of f_{st}. The value of this maximum is 30% higher than that at the station of 20 Y_j; this is due to the development of chemical-reaction as indicated by the lower value of m_{H_2} (Figure 7).

Profiles at $x/Y_j = 100$

Figure 8 shows that at a distance of 100 Y_j, the u-profile is similar to that at 60 Y_j. Also, the profiles of k and ℓ are similar to those at 60 Y_j, though the level of k is slightly lower and the maximum ℓ is higher than that at 60 Y_j.

Figure 9 displays the profiles of the species concentrations at $x/Y_j = 100$. Here the maximum value of m_{H_2}, near the wall of the centre-body, is only 15.8% of its initial value at the nozzle exit.

Comparison between Cases 1 and 2. Now the predictions of case 2 at 100 Y_j (Figures 10 and 11) are compared with those of case 1 at the same station. Both cases have the same geometry and initial conditions, except that in case 2 the initial u-velocity of the hydrogen jet is 50% larger than that in case 1.

Figure 10 shows that the u-profile is not yet fully developed; it still retains the step shape of the initial distribution. This behaviour is explained in what follows. Here, the temperature level is lower than in case 1, because the shear layer is predominatly richer in fuel than in case 1; the maximum values of f and m_{H_2} are 0.31 and 0.286 as compared to their respective values of 0.182 and 0.158 in case 1. Lower temperatures result in higher densities and hence a lower rate of velocity-decay.

4.2 The jet without a centre-body

Case 3. Figures 12 and 14 show the radial profiles of u,T, k,f,g and ℓ at two downstream-stations: x/D_j = 10 and 50. The corresponding profiles of the species mass-fractions are shown in Figures 13 and 15.

At a distance of 10 D_j downstream (Figure 12), k reaches its maximum in the high-shear region away from the axis, whereas at a distance of 50 D_j (Figure 14) where the shear flow is developed, k attains its peak at the axis. This behaviour is generally a feature of axi-symmetric jets and is different from that of the jet in cases 1 and 2 because of the presence of the centre-body.

The temperature profiles at both axial locations have their highest value where f equals f_{st}; this is also where the radicles O and OH reach their maximum concentrations (Figures 13 and 15).

Comparison between Cases 3 and 4. The profiles of u,T,k,f, g and ℓ at a downstream distance of x/D_j = 50 for case 4, are shown in Figure 16.

The profiles of the species mass-fractions at the same distance are shown in Figure 17.

The initial conditions of case 4 differ from those of case 3 only in that the static pressure of the hydrogren jet of the former is twice that of the latter. The effect of this higher pressure is seen by comparing Figures 14 and 16. It is evident that both u and f have a lower rate of decay in case 4 than in case 3; this can be attributed to the higher mass flow rate in case 4 caused by the higher pressure and density. Also the maximum mass fraction of H_2 at a distance of 50 D_j in case 4 (Figure 17) is higher than that of case 3.

4.3 The confined jet, Case 5.

Regarding case 5, the confined-flow case, it was planned to continue the integration to a downstream position of 50 D_j: however, it was not possible to proceed with the computation farther than 10 D_j, because choking was predicted there. This choking is detected by the computer program when the calculated flow-area necessary to satisfy the conservation of lateral momentum exceeds that required for conservation of mass (here this is equal to the area of the confining duct). This situation indicates that the intitial flow conditions for case 5 are not compatible with the flow through the duct.

It is suggested that new initial conditions should be specified for this case, e.g. by successively lowering the velocity of the hydrogen jet, and performing further runs.

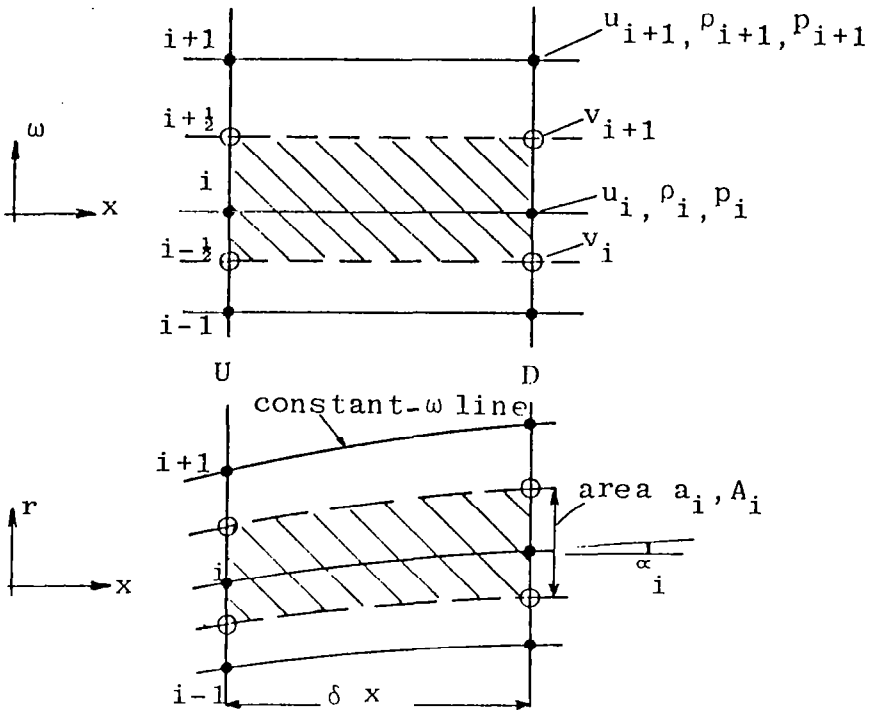

Figure 1: The finite-difference grid in both the x-ω and the x-r coordinates.

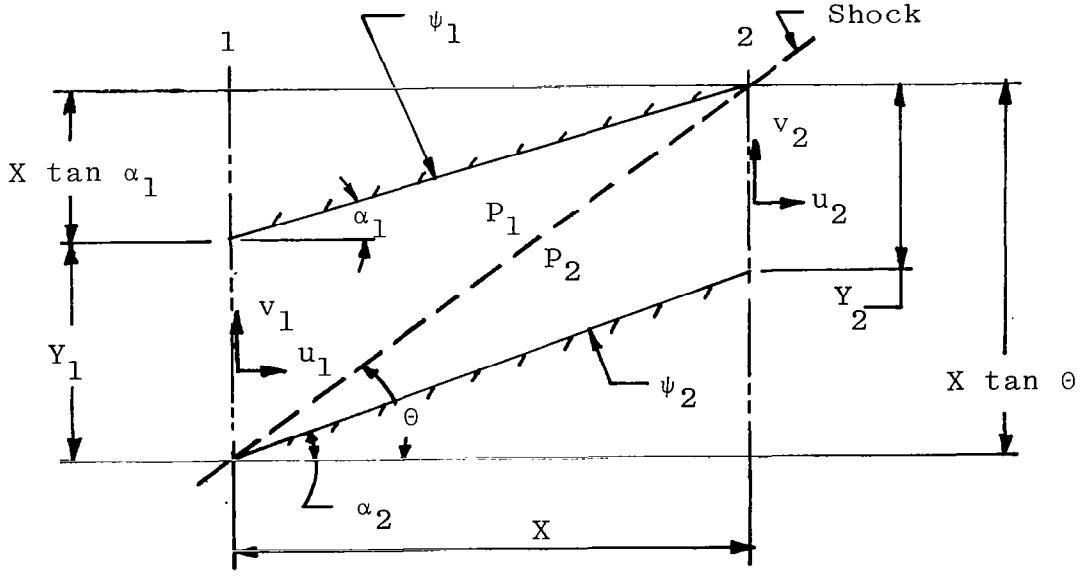

Figure 2: Definition of Notations

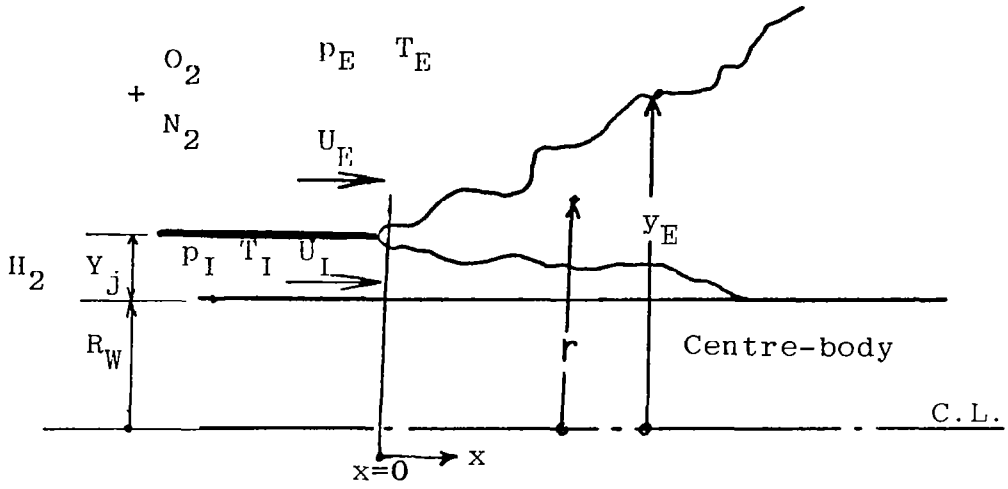

a - Cases 1 and 2

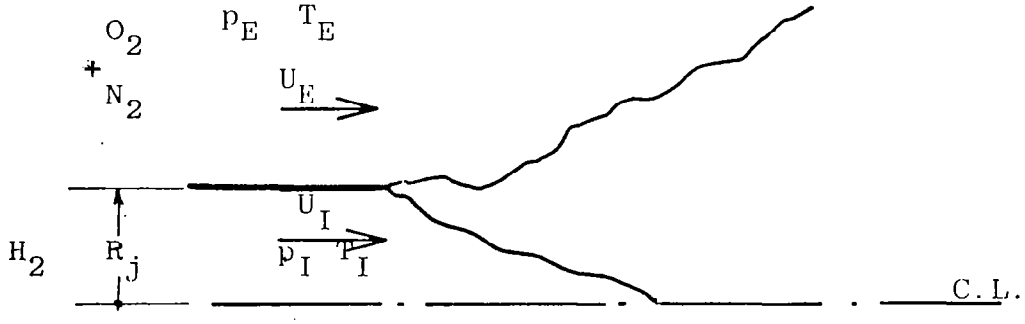

b - Cases 3 and 4

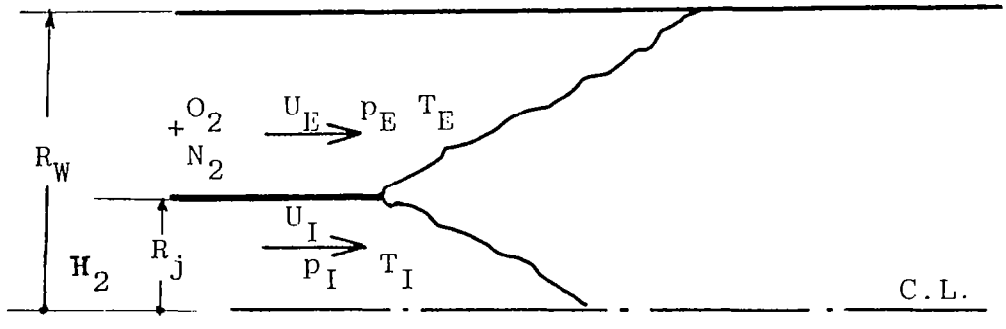

c - Case 5

Figure 3 : The Flow Geometry of the Five Test Cases

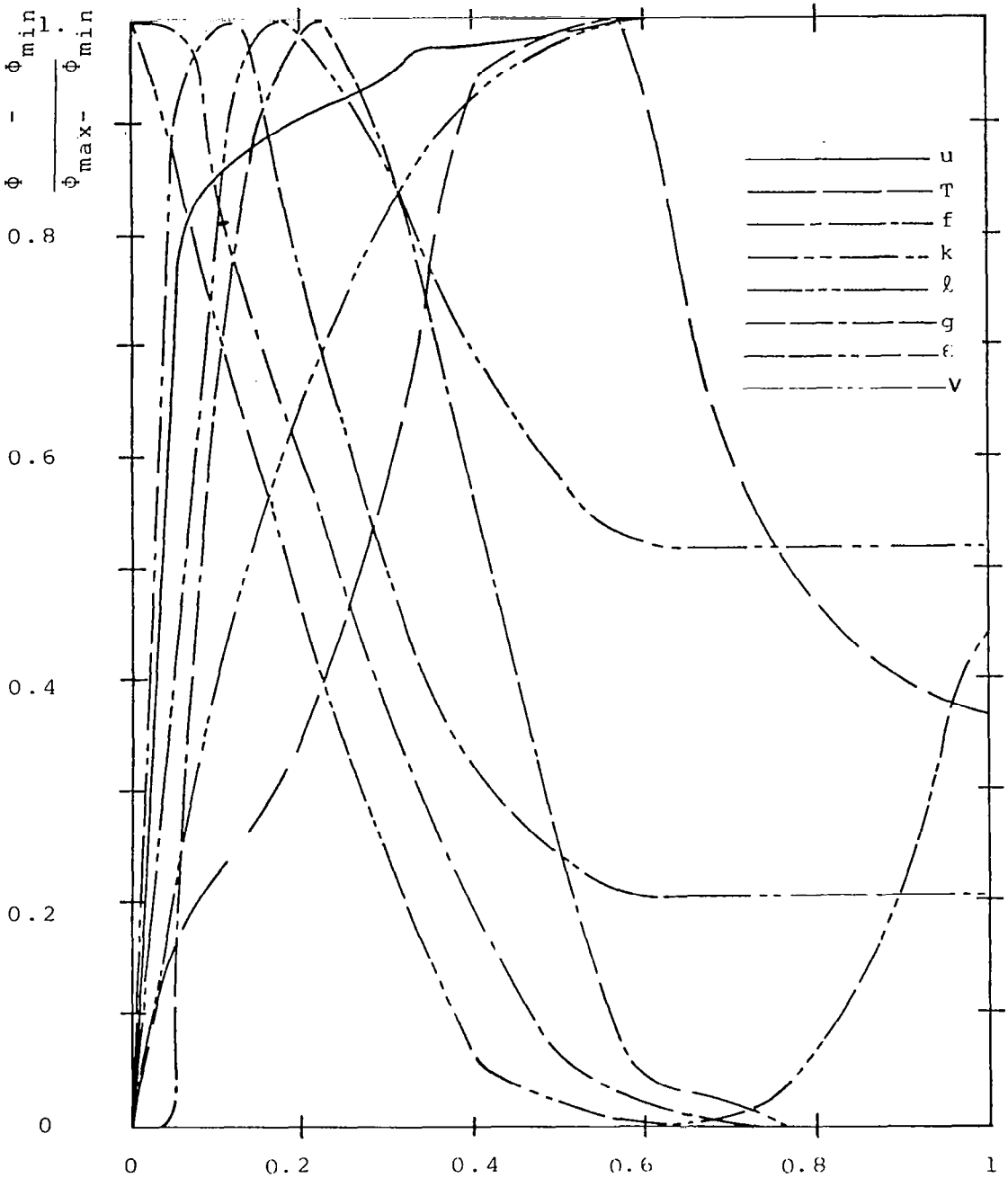

Fig.4 Radial profiles of u,T,k,ε,f,g,ℓ and v at x/Y_j=20; Case 1.

Φ	Φ_{max}	Φ_{min}	Φ	Φ_{max}	Φ_{min}
u	1804	0.	f	0.509	0.
T	1889	300	g	0.07	0.
k	2.4×10^4	0.	ℓ	0.016	0.
ε	4.8×10^8	0.	v	0.	-11.9

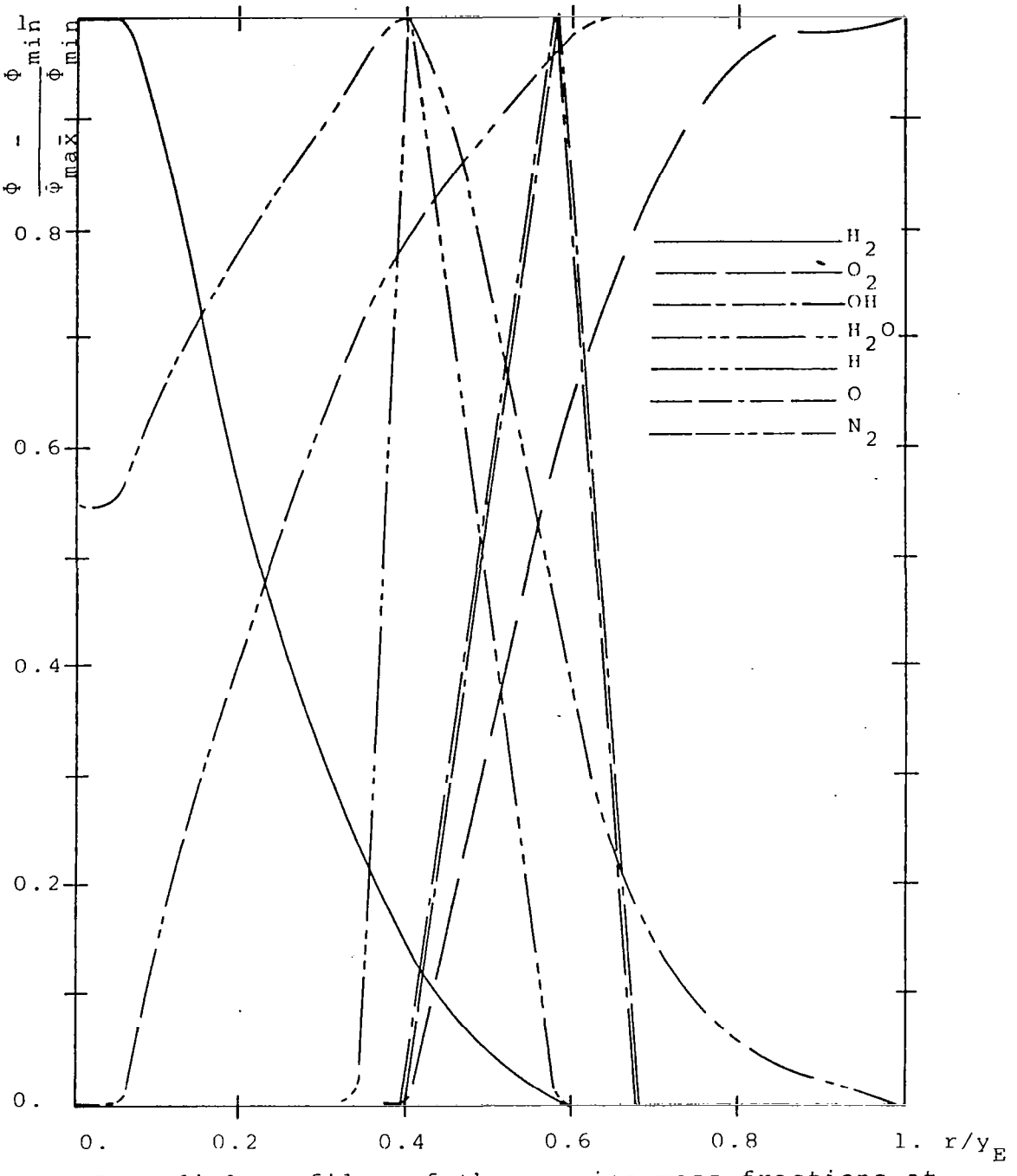

Fig. 5. Radial profiles of the species mass-fractions at $x/Y_j = 20$, Case 1.

Φ	Φ max	Φ min	Φ	Φ max	Φ min
H_2	0.495	0.	H	1.70×10^{-5}	0.
O_2	0.232	0.	O	7.74×10^{-5}	0.
OH	7.28×10^{-4}	0.	N_2	0.768	0.37
H_2O	0.234	0.			

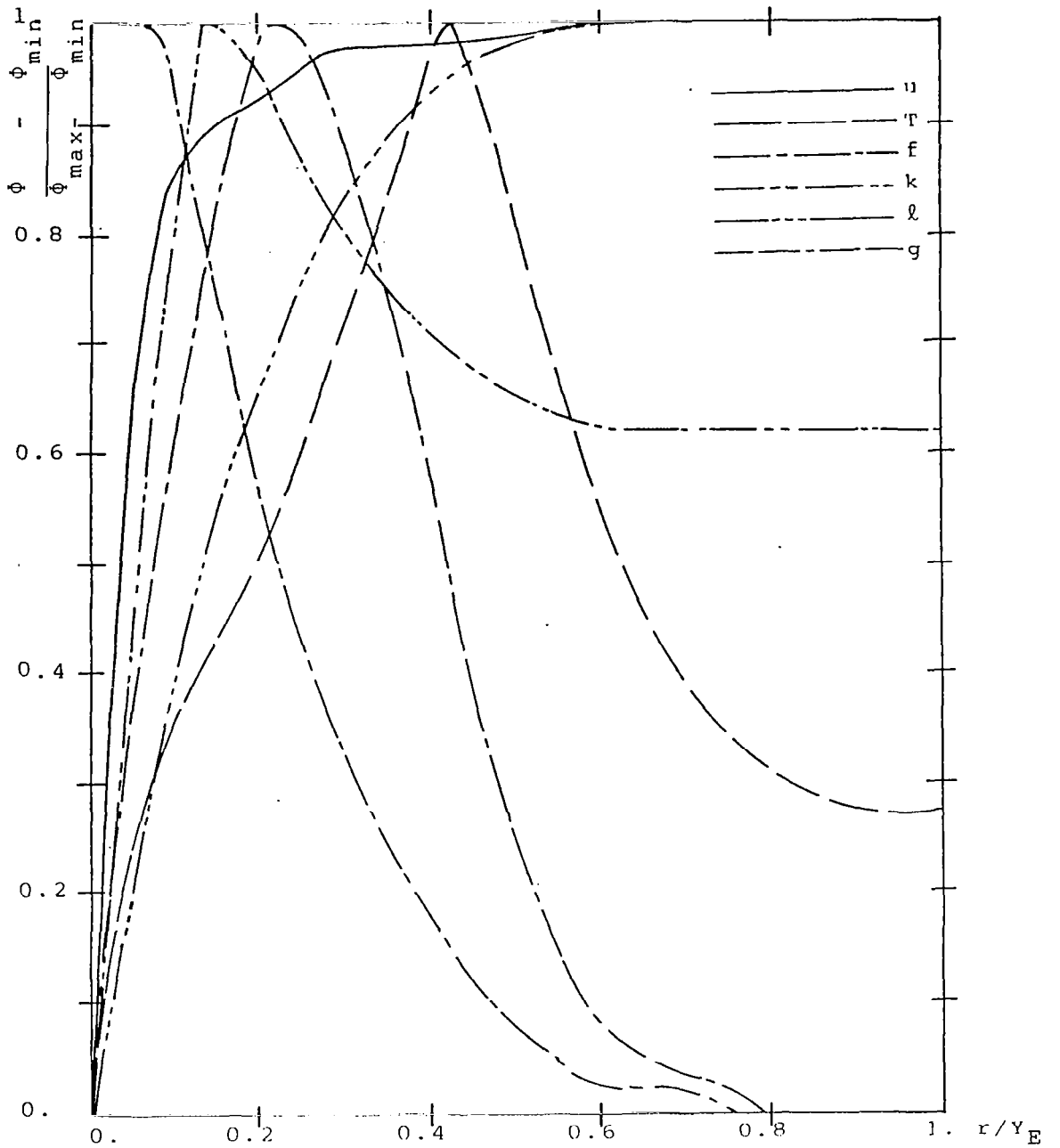

Fig.6 Radial profiles of u,T,k,f,g and ℓ at $x/Y_j = 60$, Case 1.

Φ	Φmax	Φ min	Φ	Φ max	Φmin
u	1801	0.	f	0.265	0.
T	2523	300	g	0.0175	0.
k	1.46×10^4	0.	ℓ	0.0187	0.

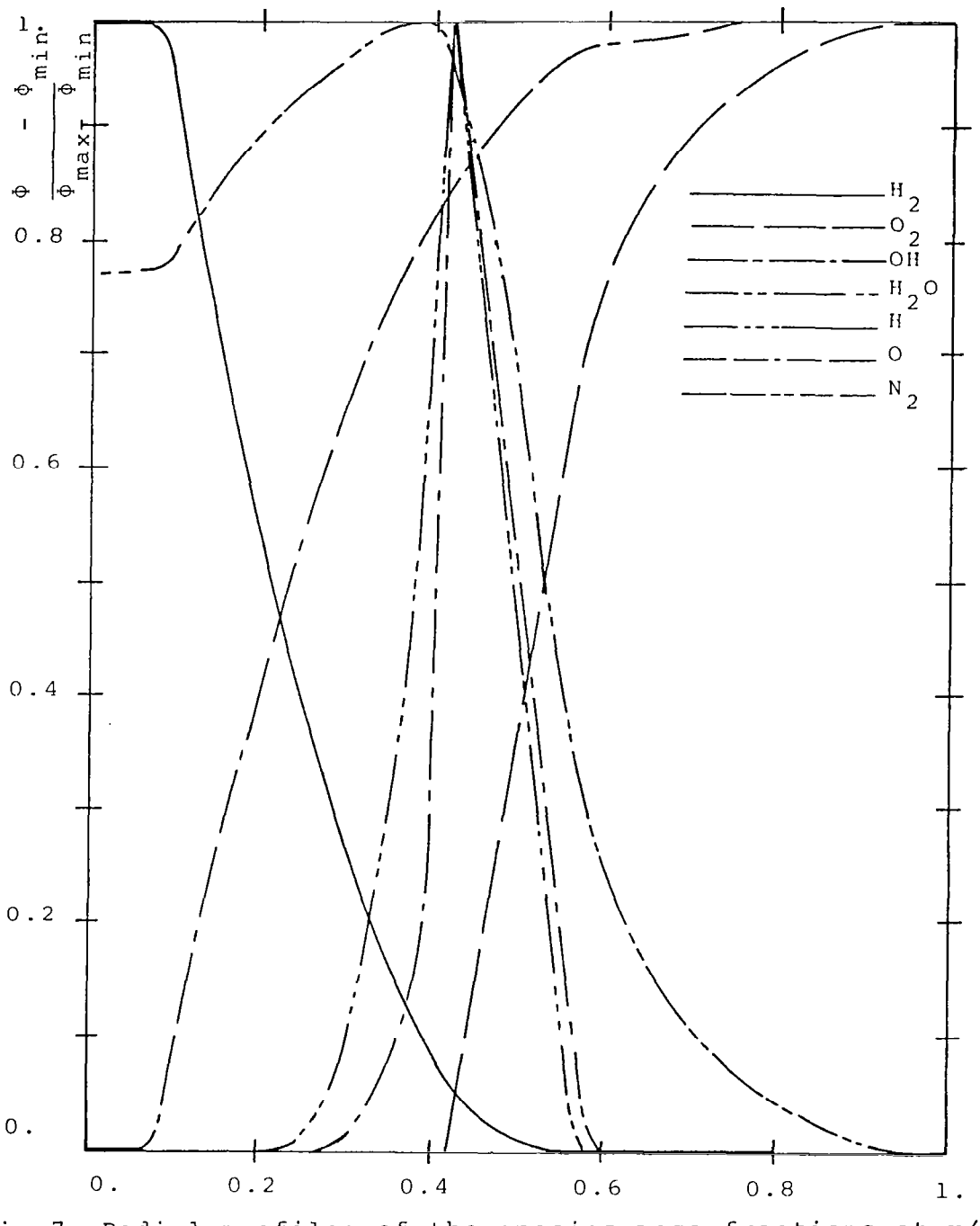

Fig.7 Radial profiles of the species mass-fractions at x/y_j= 60, Case 1.

Φ	Φ max	Φ min	Φ	Φ max	Φ min
H_2	0.244	0.	H	4.48×10^{-4}	0.
O_2	0.232	0.	O	1.71×10^{-4}	0.
OH	3.75×10^{-3}	0.	N_2	0.768	0.565
H_2O	0.245	0.			

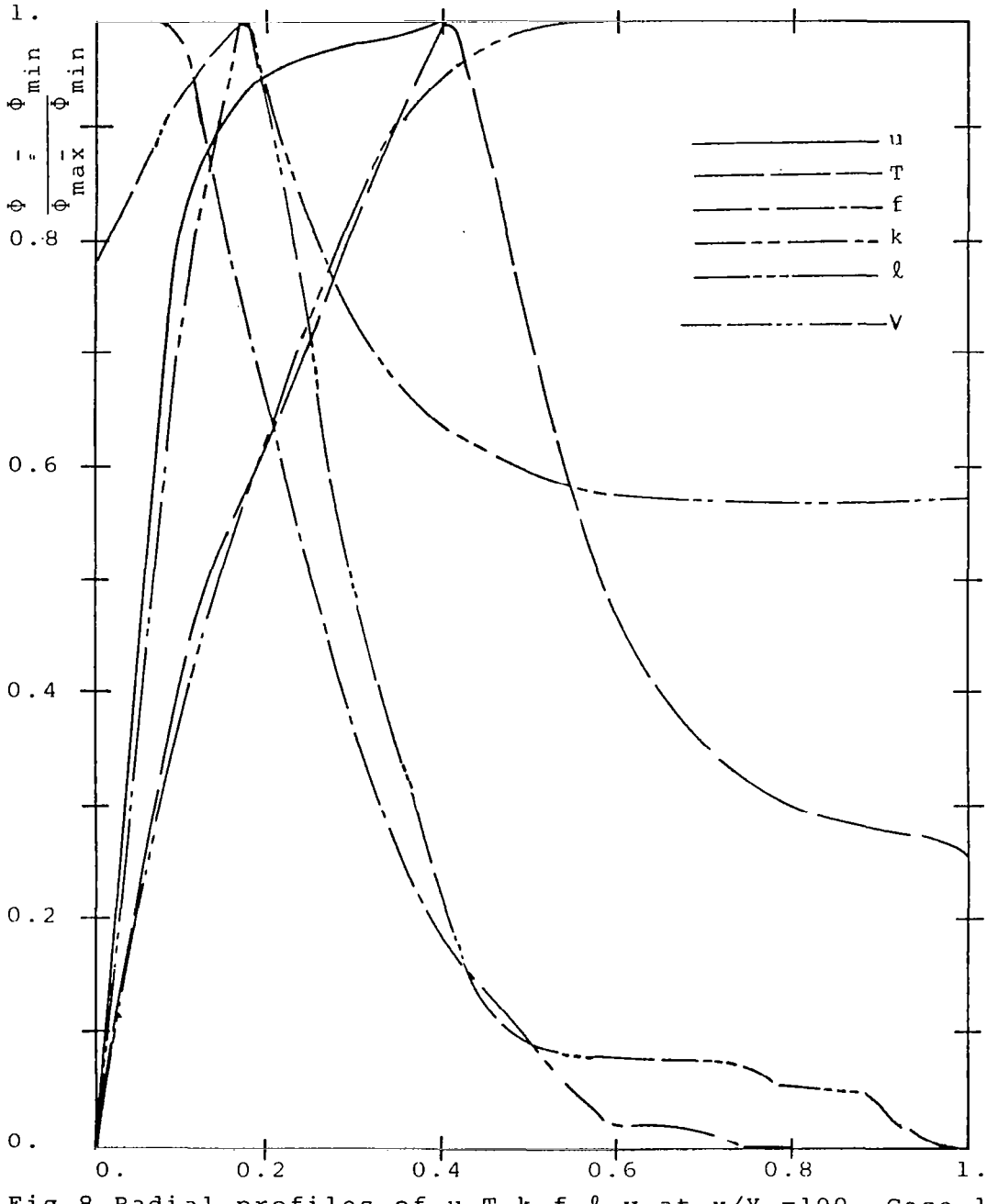

Fig.8 Radial profiles of u,T,k,f,ℓ,v at x/Y_j=100, Case 1.

Φ	Φ max	Φ min	Φ	Φ max	Φ min
u	1800	0.	f	0.182	0.
T	2592	300	ℓ	0.021	0.
k	1.2×10^4	0.	v	0.224	-0.79

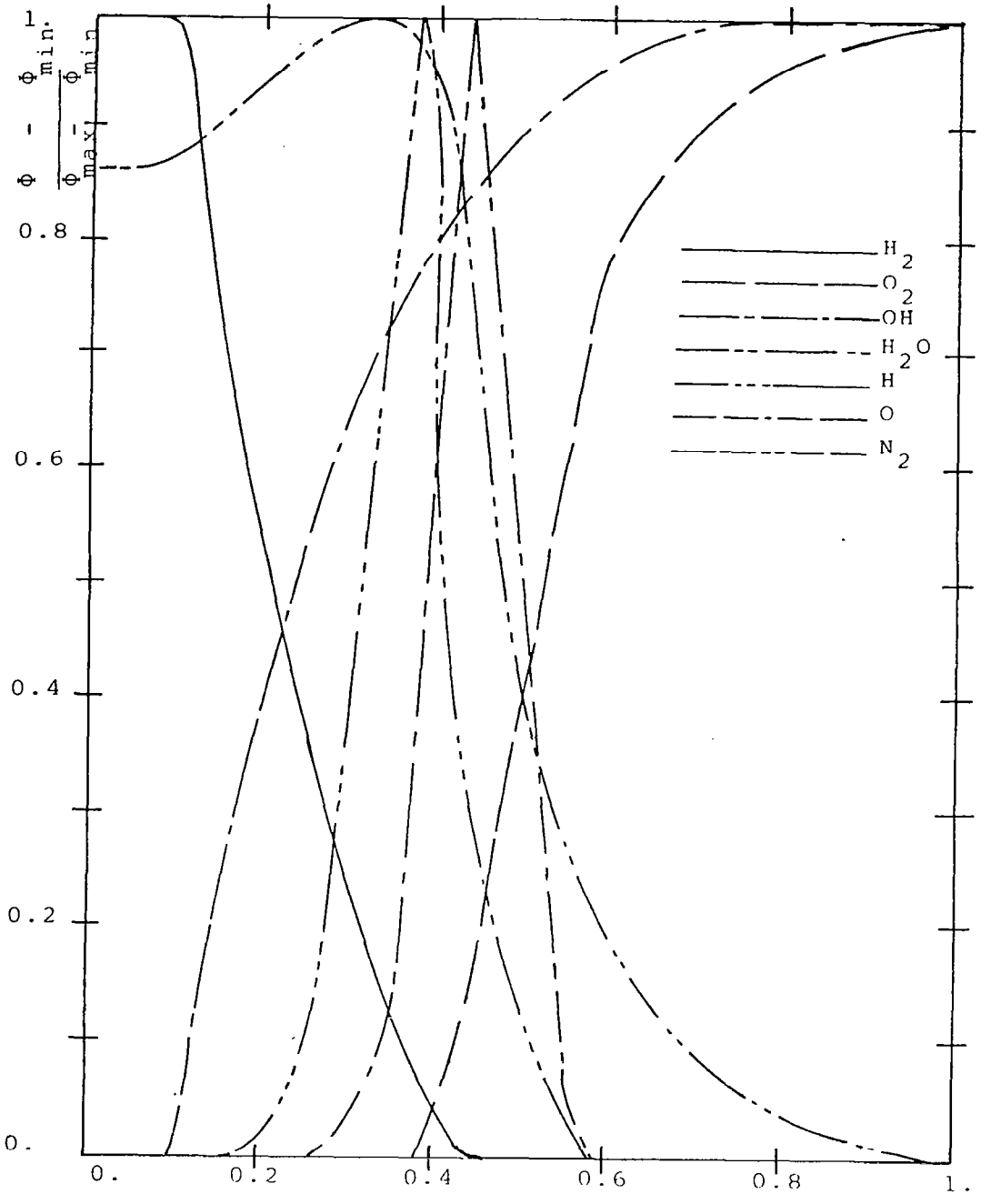

Fig.9 Radial profiles of the species mass-fraction at x/Y_j = 100, Case 1.

Φ	Φ max	Φ min	Φ	Φ max	Φ min
H_2	0.158	0.	H	4.41×10^{-4}	0.
O_2	0.232	0.	O	.0016	0.
OH	0.011	0.	N_2	0.768	0.628
H_2O	0.245	0.			

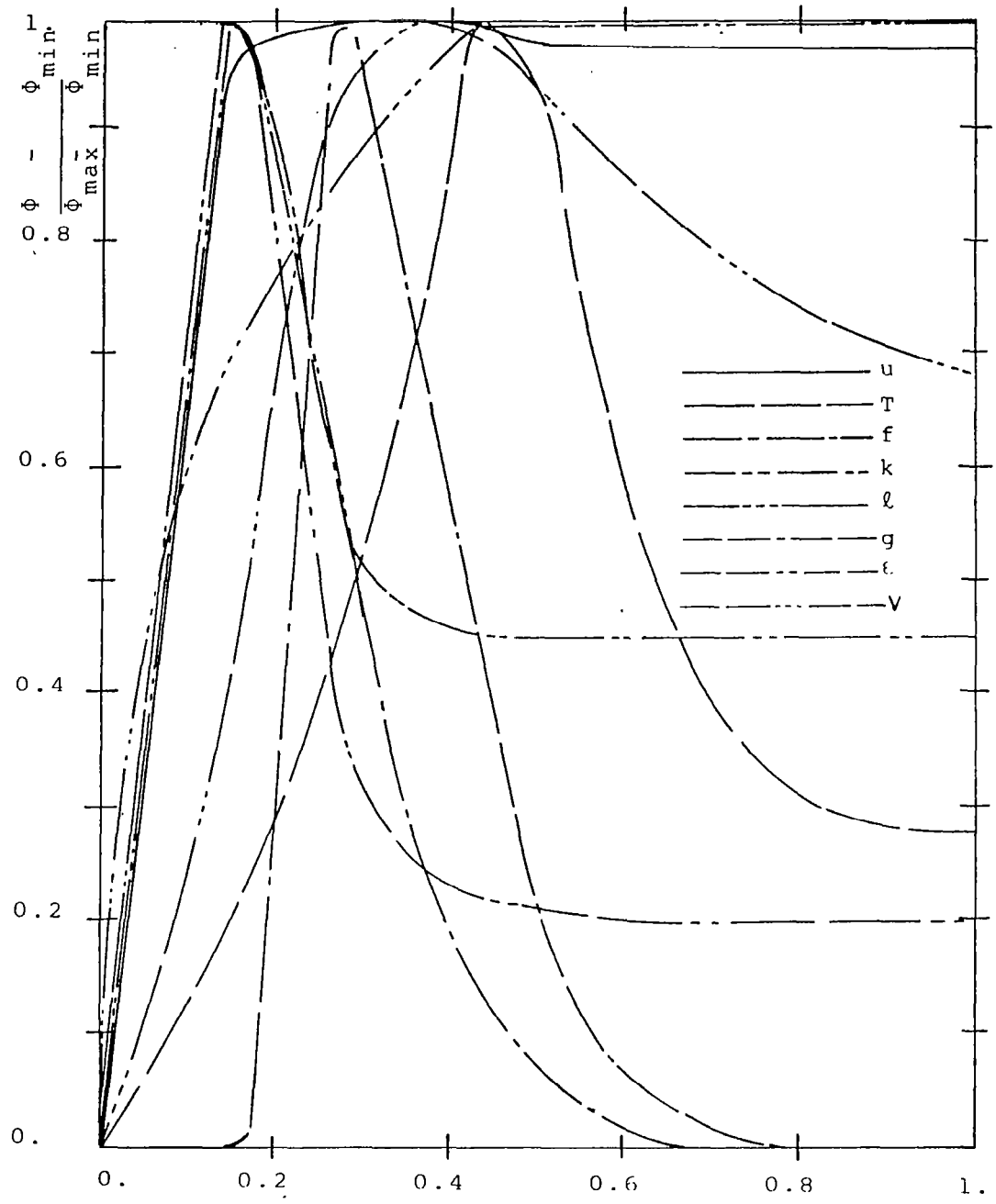

Fig. 10. Radial profiles of u,T,k,ε,f,g,ℓ,v at x/Y_j = 100, Case 2.

Φ	Φ max	Φ min	Φ	Φ max	Φ min
u	1832	0.	f	0.31	0.
T	2454	300	g	0.021	0.
k	1.6×10^{4}	0.	ℓ	0.021	0.
ε	1.3×10^{8}	0.	v	3.35	0.

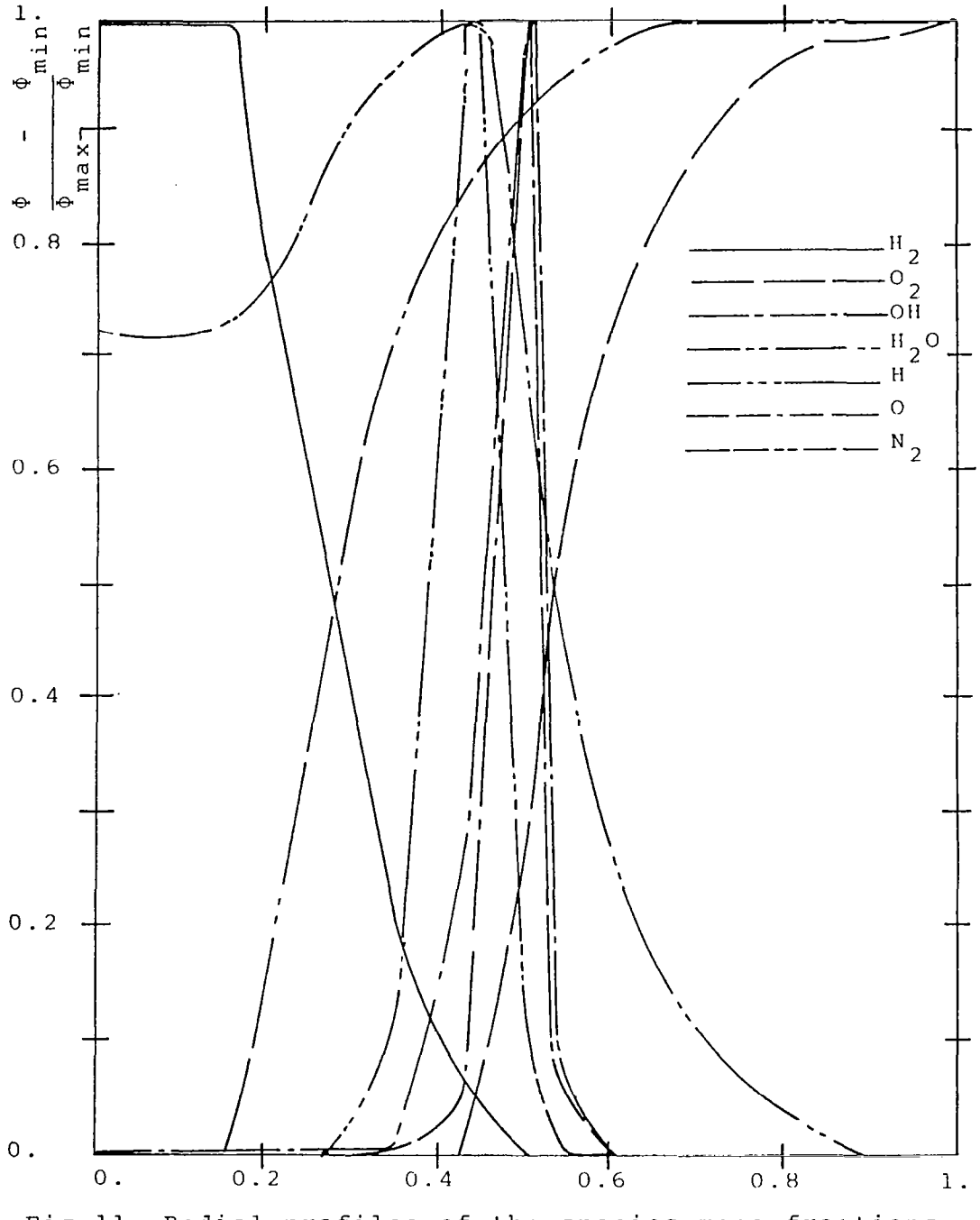

Fig.11 Radial profiles of the species mass-fractions

Φ	Φ max	Φ min	Φ	Φ max	Φmin
H_2	0.286	0.	H	3.6×10^{-4}	0.
O_2	0.232	0.	O	0.001	0.
OH	0.0077	0.	N_2	0.768	0.533
H_2O	0.245	0.			

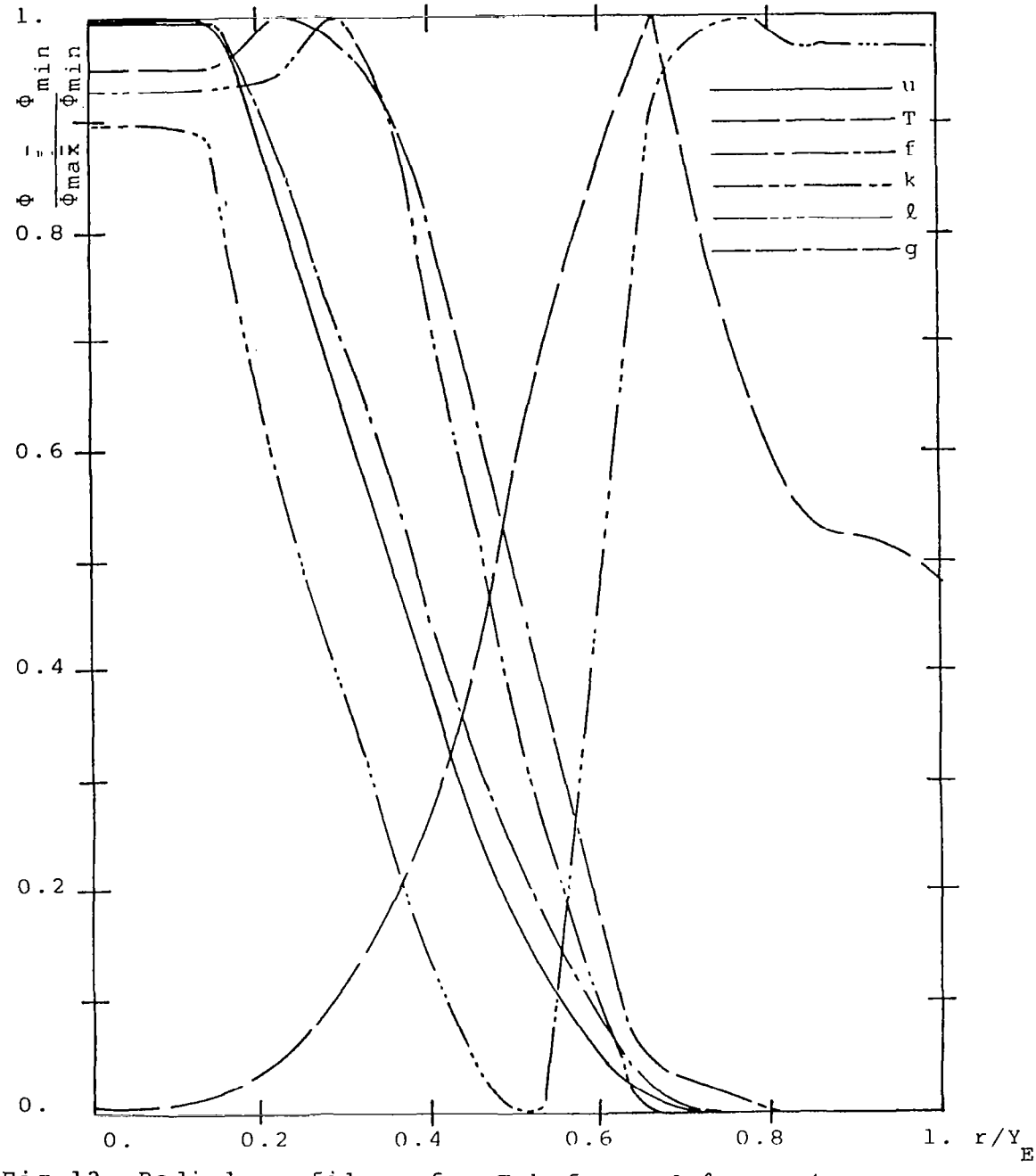

Fig.12 Radial profiles of u,T,k,f,g and ℓ at x/D_j=10,Case 3.

Φ	Φ max	Φ min	Φ	Φ max	Φ min
u	2089	1427	f	0.605	0.
T	2520	470	g	0.05	0.
k	4.55×10^4	5.41×10^3	ℓ	0.0052	0.0036

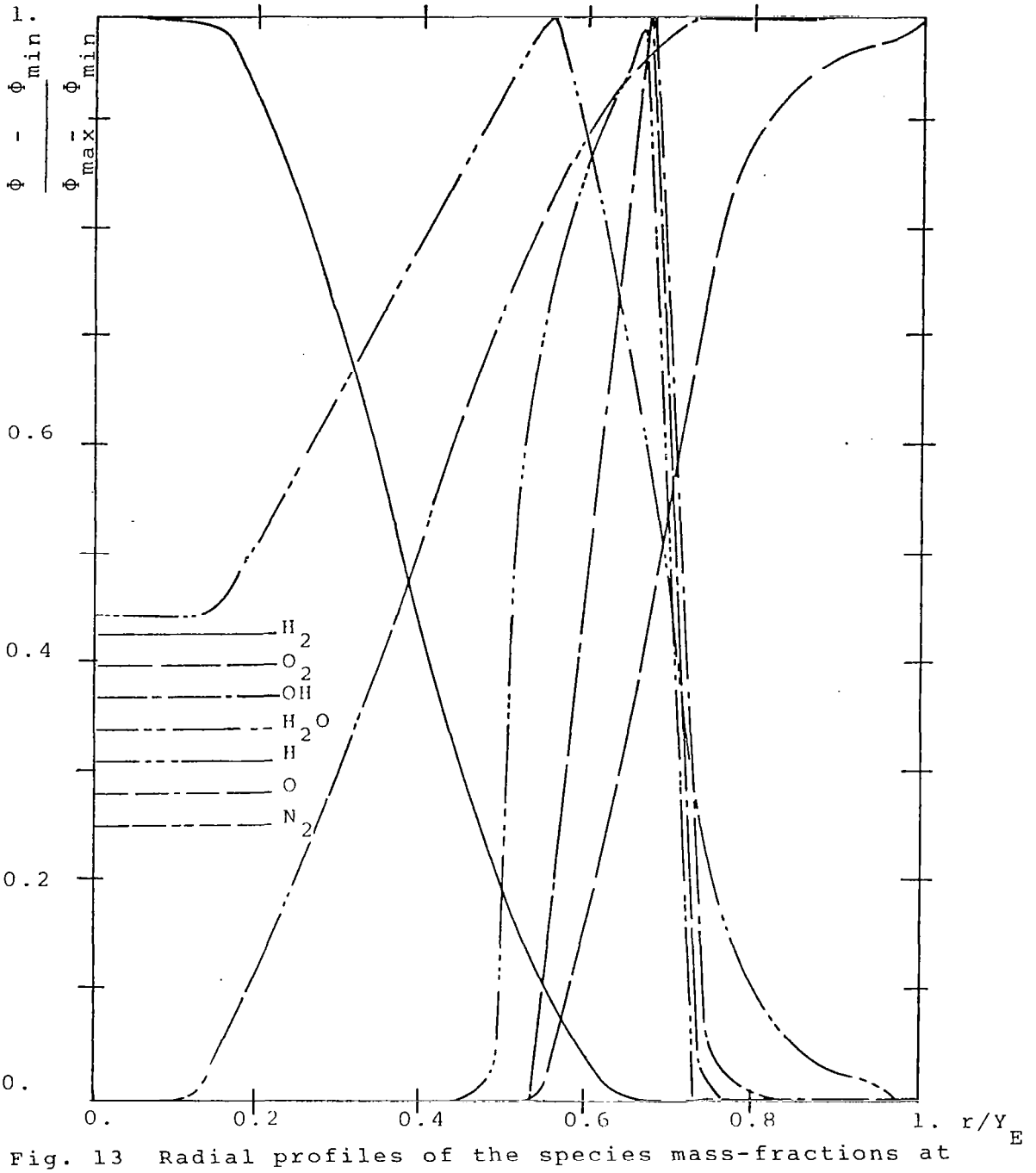

Fig. 13 Radial profiles of the species mass-fractions at x/D_j = 10, Case 3.

Φ	Φ max	Φ min	Φ	Φmax	Φmin
H_2	0.594	0.	H	7.4×10^{-5}	0.
O_2	0.232	0.	O	0.0026	0.
OH	0.011	0.	N_2	0.768	0.303
H_2O	0.234	0.			

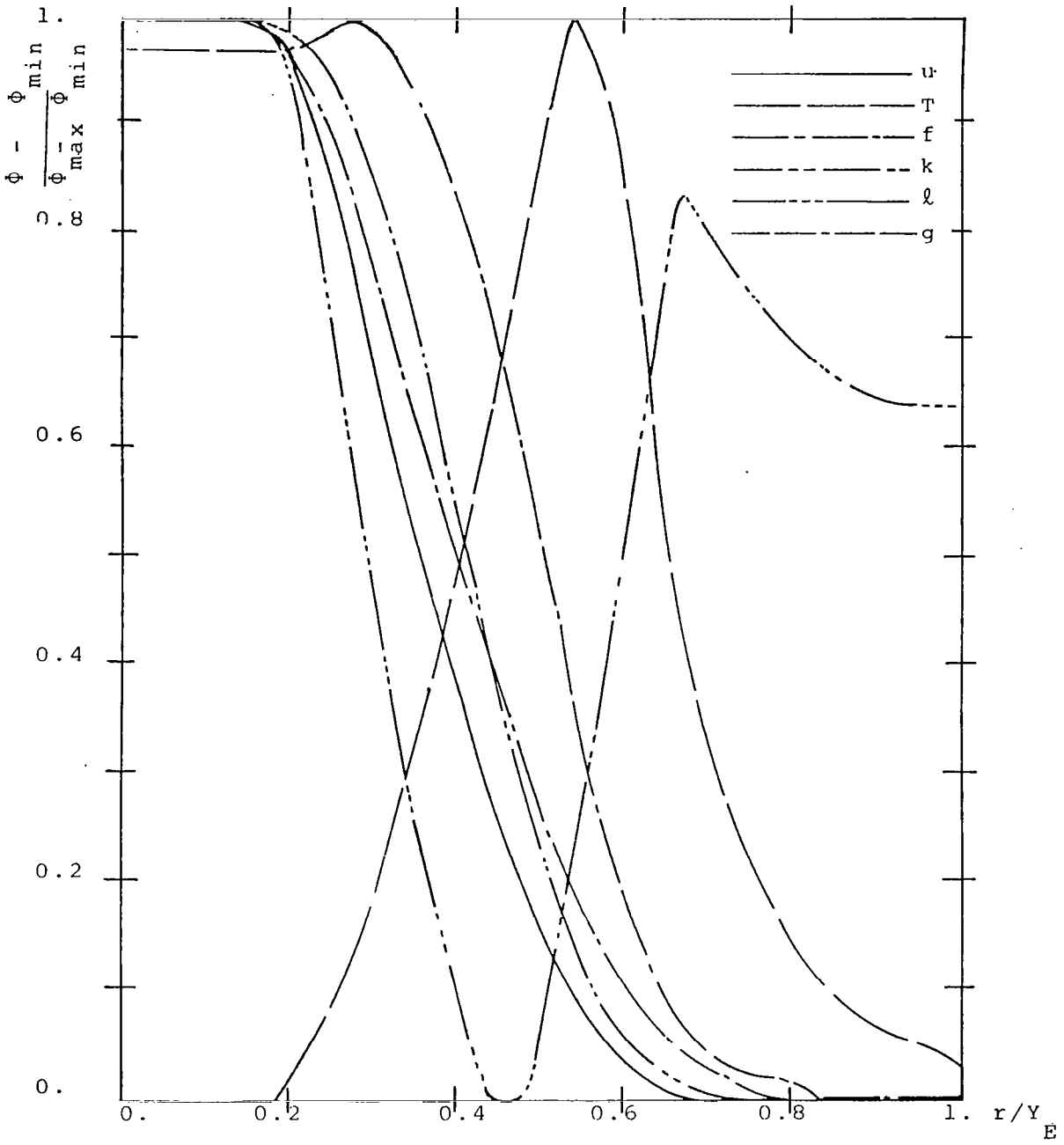

Fig.14 Radial profiles of u,T,k,f,g and ℓ at x/D_j = 50, Case 3.

Φ	Φ max	Φ min	Φ	Φ max	Φ min
u	1650	1431	f	0.176	0.
T	2464	1424	g	0.0058	0.
k	1.14×10^4	1.86×10^3	ℓ	0.0092	0.0076

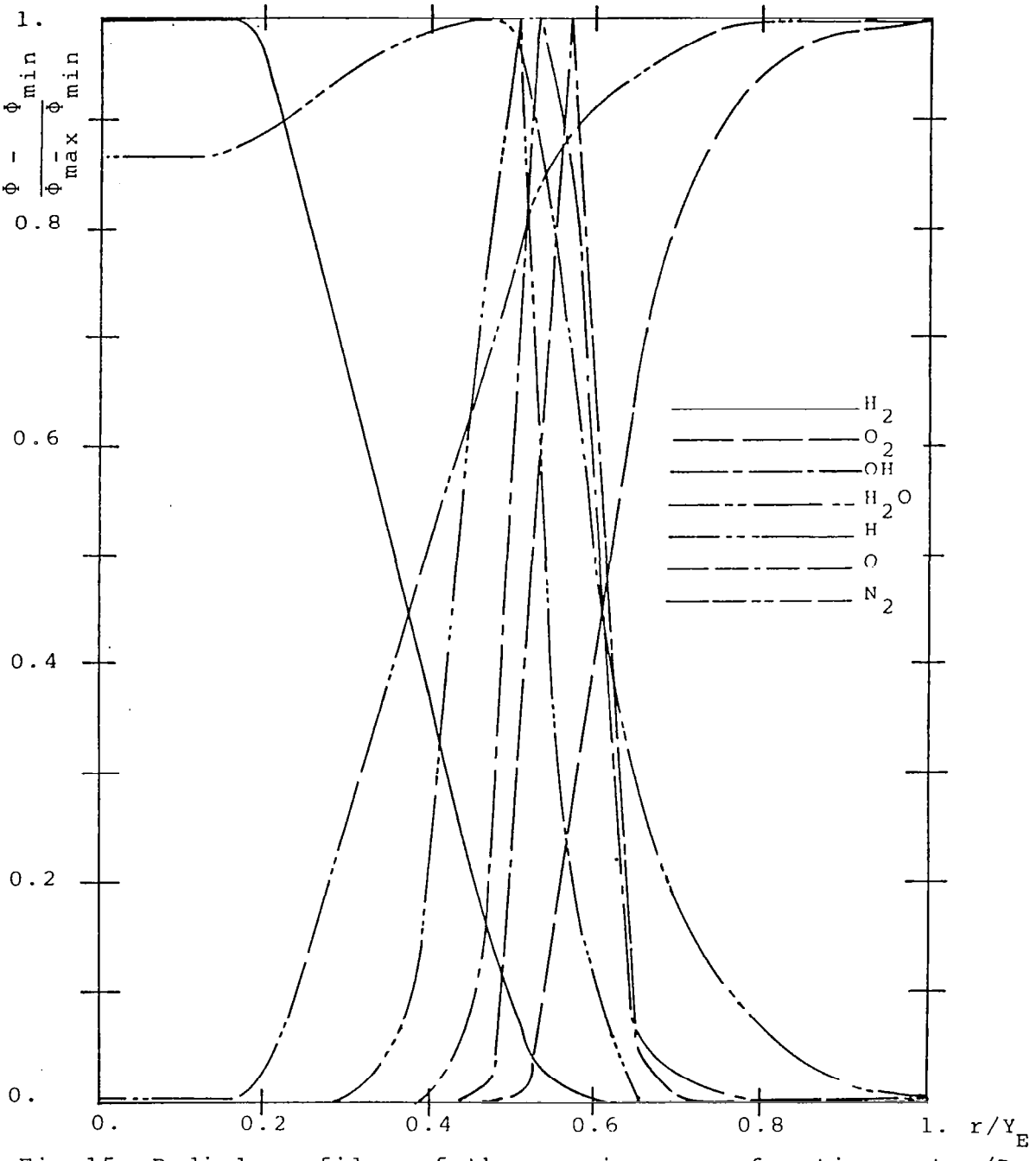

Fig.15 Radial profiles of the species mass fractions at $x/D_j = 50$

Φ	Φ max	Φ min	Φ	Φ max	Φmin
H_2	0.1525	0.	H	9.5×10^{-4}	0.
O_2	0.232	0.	O	3.55×10^{-3}	0.
OH	0.017	0.	N_2	0.768	0.632
H_2O	0.242	0.			

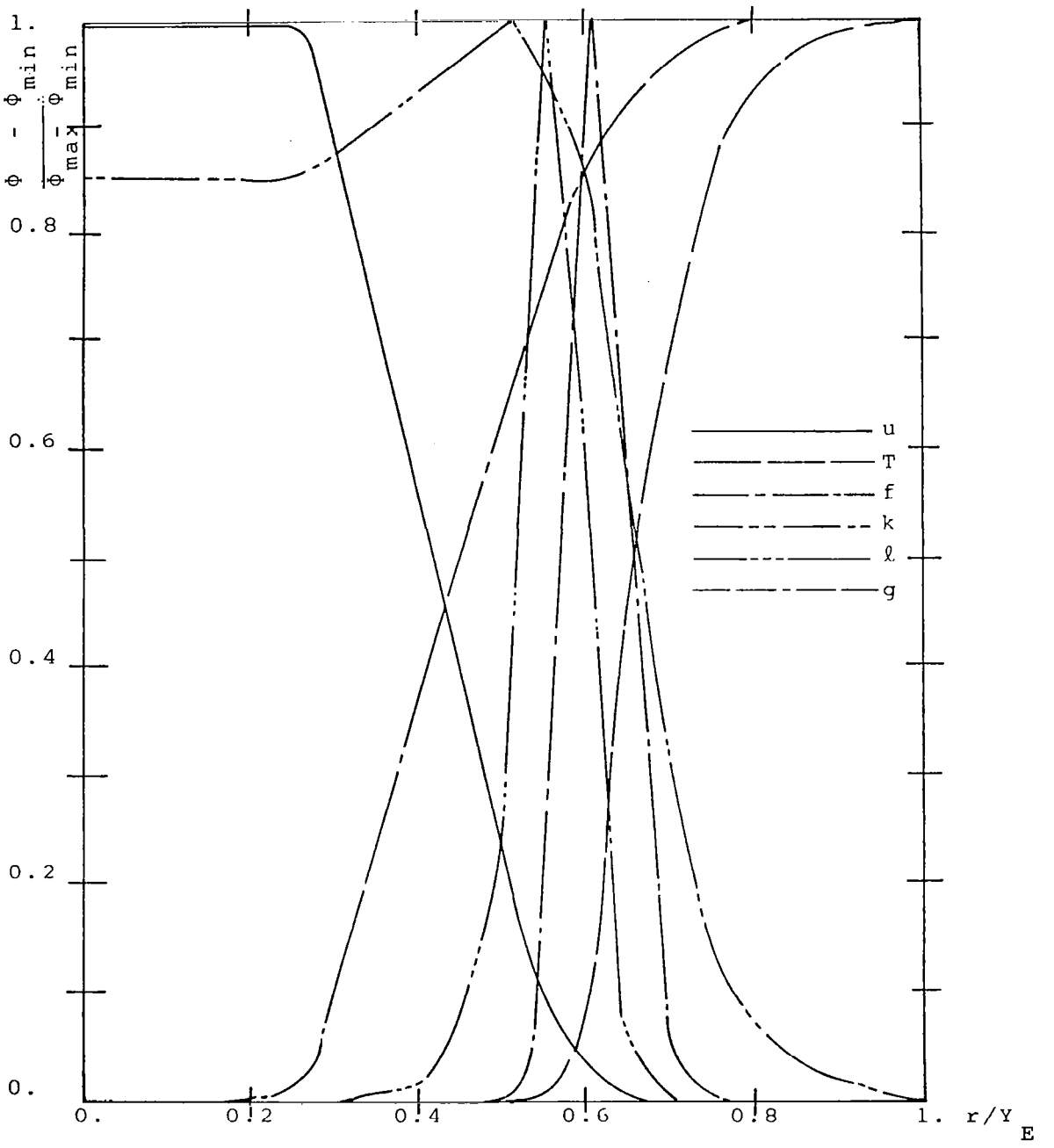

Fig.16 Radial profiles of u,T,k,f,g and ℓ at x/D_j = 50, Case 4.

Φ	Φ max	Φ min	Φ	Φ max	Φmin
u	1761	1430	f	0.21	0.
T	2734	1210	g	0.0076	0.
k	2.16×10^4	1.85×10^3	ℓ	0.01	0.008

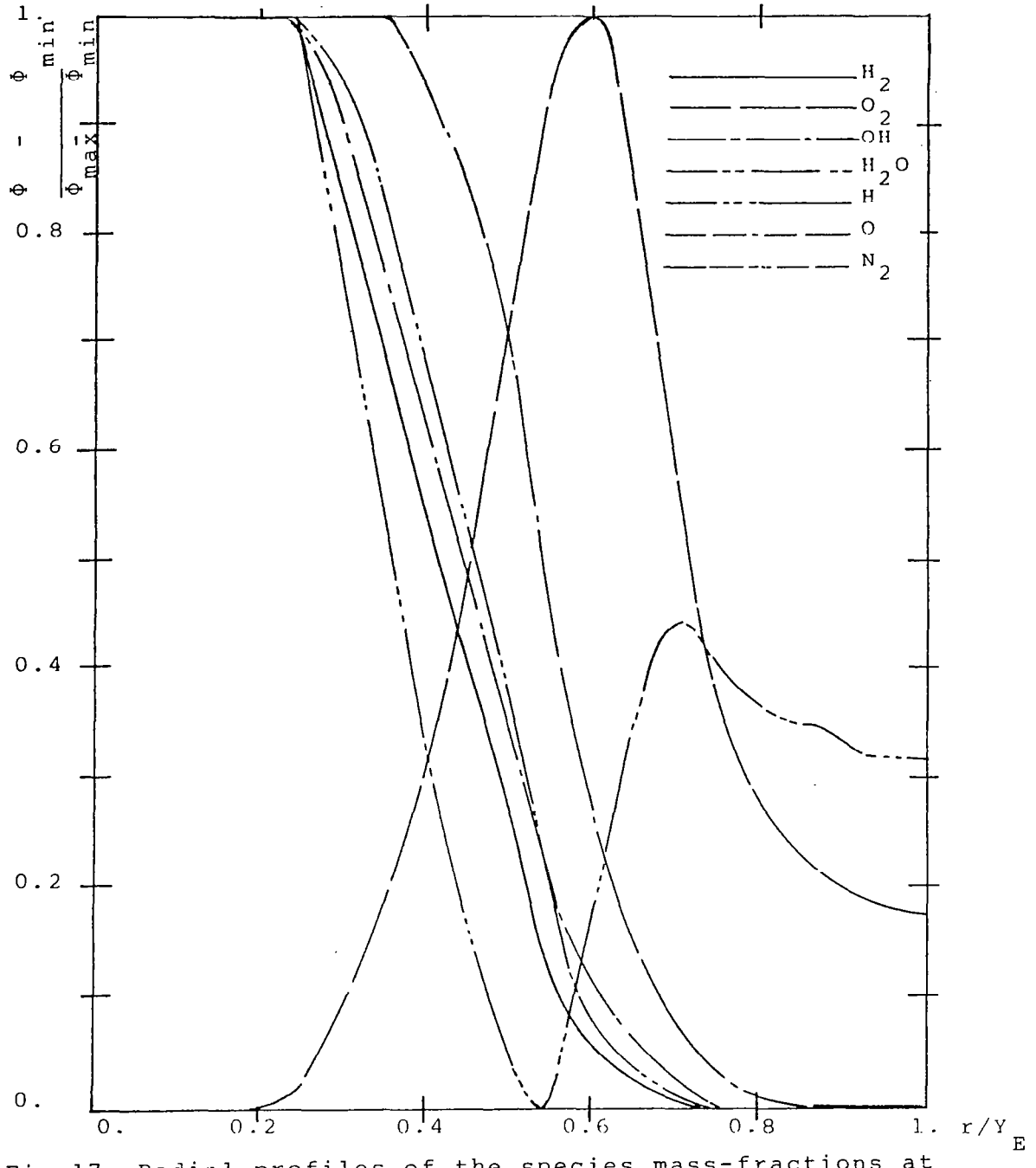

Fig.17 Radial profiles of the species mass-fractions at $x/D_j=50$, Case 4.

Φ	Φ	Φ	Φ	Φ	Φ
H_2	0.191	0.	H	8.72×10^{-4}	0.
O_2	0.232	0.	O	3.7×10^{-3}	0.
OH	0.018	0.	N_2	0.768	0.604
H_2O	0.241	0.			

5. SUGGESTIONS FOR FURTHER EXTENSIONS AND REFINEMENTS OF ALMA

The following extensions and refinements to ALMA are easily possible; and they may prove to be necessary when the predictions of ALMA are compared with experimental data:-

(a) Introduction of realistic chemistry

As has been explained, thermodynamic equilibrium has been postulated in ALMA; the chemical reaction rates have been presumed to be very fast. The presumption is at best an approximation to the truth; and it will undoubtedly be necessary, from time to time, to examine how the predictions will change if chemical-kinetic limitations are allowed for.

These limitations may be of two kinds: those associated with the chemical kinetics of laminar-flow processes; or those concerned with "eddy break up". New ideas (Ref.2) concerning the interactions of these two modes are now available; and the ALMA code can be easily extended to accommodate these ideas.

The extension naturally takes the form of the provision and solution of further differential equations, together with auxiliary relations concerning sources. However, in order that the associated computer time does not become excessive, simultaneous improvements in the numerical procedures discovered since ALMA was conceived, may be advantageously introduced.

(b) Introduction of "partially-parabolic" effects

ALMA is an advance over CHARNAL, in that it takes account of the lateral-momentum effects in the supersonic-flow regions. However, where the flow is subsonic, the variation of pressure with radius has to be ignored if the marching nature of the integration is to be preserved.

In some circumstances, the inaccuracies resulting from this practice are not to be tolerated. Fortunately, experience now exists of handling the lateral-momentum effects in subsonic regions by the so-called "partially-parabolic" method (Ref. 7). It is true that repeated marching integrations must be made, to this end; so computer time increases. However, the partially-parabolic method is economical of storage: only the pressure has to be stored for the whole two-dimensional flow field; so the storage requirement is scarcely greater than that of ALMA.

(c) Allowance for small patches of recirculation.
In a still further extension, "elliptic" flow regions may be incorporated. These require still further storage. However, recent coding developments (Ref. 8) have permitted the additional storage, and the more numerous iterations, to be restricted to the regions of recirculation themselves. It is not necessary, just because shock-wave-boundary-layer separation occurs in one area, to forego entirely the economies associated with marching integration.

This refinement will also be important if it should become important to compute the influence of the finite thickness of the "lip" of the hydrogen-injection nozzle.

Of course, the stream-line coordinate system must be abandoned, at least in the recirculation region. However, means exist of retaining its advantages elsewhere.

APPENDIX A. Symbols

A	cross-sectional flow area of a control volume in the continuity equation;
a	cross-sectional flow area of a control volume in the lateral momentum equation;
C	coefficients in the pressure correction equation;
$C_\mu, C_1, C_2, C_{g1}, C_{g2}$	constants coefficients appearing in turbulence model;
c_l	speed of sound;
$c_{p,j}$	mean specific heat of species j;
D_j	diameter of jet nozzle;
F	mixture fraction of elemental oxygen;
f	mixture fraction or mass fraction of elemental hydrogen;
f_{st}	stoichiometric value of f;
g	mean square fluctuations of f ($\equiv \overline{f'^2}$):
h	enthalpy;
$H_{j,T_{ref}}$	heat of formation of species j at $T = T_{ref}$
$\tilde{h}$	stagnation enthalpy;
K_p	general equilibrium constant;
K_i	equilibrium constant for the reaction i;
K_i'	modified equilibrium constant;
k	kinetic energy of turbulence;
ℓ	length scale of turbulence = $k^{3/2}/\varepsilon$;
m_j	mass fraction of species j

p	static pressure;
r	radius (measured from axis of jet);
R_j	radius of hydrogen pipe at exit;
R_w	radius of duct enclosing the jets or radius of center-body;
T	Temperature;
u	axial component of velocity (along a constant-ω line);
v	radial component of velocity;
W	average molecular weight of the mixture;
W_j	molecular weight of j species;
x	distance along axis of jet;
X_j	mole fraction of species j;
y	radial distance (measured from axis of jet);
Y_E	radius of the outer edge of the jet
Y_j	width of the annulus of the hydrogen jet;

Greek Symbols

Symbol	
α	angle between the constant-ω line and axis of jet;
γ	the ratio of specific heats;
θ	angle between a streamline and axis of jet;
ε	rate of turbulence energy dissipation;
ρ	density;
ϕ	general variable;
Ψ	stream function;
ω	non-dimensional stream function;

Superscripts

Symbol	
*	estimated quantity;
'	correction component except in the definitions of the chemical equilibrium constants.

APPENDIX B. Table of Equilibrium Constants

Temp.	K_1'	K_2'	K_3'	K_4'	$\bar{A}$	$\bar{B}$	$\bar{C}$	$\bar{D}$
200	5.0+100	3.1E+99	2.6+100	2.6+100	4.4E-51	1.7E-50	2.42E+50	1.95E+00
400	2.8E+52	2.7E+58	3.2E+51	6.2E+59	5.9E-27	6.0E-30	4.3E+29	2.19E+04
600	2.3E+33	4.3E+36	5.8E+32	9.0E+37	2.0E-17	4.7E-19	1.09E+19	8.46E+02
800	5.9E+23	4.9E+25	2.2E+23	9.3E+26	1.2E-12	1.4E-13	4.95E+13	1.56E+02
1000	9.7E+17	1.2E+19	4.5E+17	2.2E+20	1.0E-09	2.7E-10	2.94E+10	5.94E+01
1200	1.2E+14	5.0E+14	7.0E+13	8.2E+15	8.7E-08	4.4E-08	2.14E+08	3.14E+01
1400	2.1E+11	3.5E+11	1.2E+11	5.4E+12	2.1E-06	1.6E-06	5.22E+06	1.81E+01
1600	1.7E+09	1.1E+09	1.1E+09	2.2E+10	2.4E-05	2.5E-05	3.67E+05	1.32E+01
1800	3.9E+07	2.1E+07	2.7E+07	3.0E+08	1.5E-04	2.1E-04	4.53E+04	9.45E+00
2000	1.9E+06	7.0E+05	1.4E+06	9.8E+06	7.2E-04	1.1E-03	8.63E+03	7.76E+00
2200	1.5E+05	4.3E+04	1.2E+05	5.8E+05	2.5E-03	4.8E-03	2.24E+03	6.96E+00
2400	1.9E+04	4.2E+03	1.6E+04	5.5E+04	7.0E-03	1.5E-02	0.71E+03	5.77E+00
2600	3.4E+03	5.8E+02	2.8E+03	7.6E+03	1.7E-02	4.1E-02	2.6E+02	5.30E+00
2800	7.5E+02	1.0E+02	6.4E+02	1.3E+03	3.6E-02	9.6E-02	1.11E+02	4.49E+00
3000	2.0E+02	2.4E+01	1.74+02	3.1E+02	7.0E-02	2.0E-01	5.37E+01	4.37E+00
3200	6.3E+01	6.8E+00	5.7E+01	8.5E+01	1.2E-01	3.8E-01	2.95E+01	3.87E+00
3400	2.3E+01	2.1E+00	2.1E+01	2.7E+01	2.0E-01	6.7E-01	1.70E+01	3.62E+00
3600	9.3E+01	7.9E-01	8.6E+00	9.8E+00	3.2E-01	1.1E+00	1.02E+01	3.45E+00
3800	4.1E+00	3.2E-01	3.8E+00	3.9E+00	4.9E-01	1.7E+00	6.38E+00	3.25E+00
4000	1.9E+00	1.4E-01	1.8E+00	1.7E+00	7.0E-01	2.6E+00	4.30E+00	3.09E+00
4200	1.0E+00	6.8E-02	9.8E-01	8.3E-01	9.8E-01	3.8E+00	3.12E+00	3.09E+00
4400	5.5E-01	3.5E-02	5.4E-01	4.2E-01	1.3E+00	5.3E+00	2.20E+00	2.89E+00
4600	3.2E-01	1.8E-02	3.1E-01	2.2E-01	1.7E+00	7.2E+00	1.59E+00	2.69E+00
4800	1.9E-01	1.0E-02	1.9E-01	1.3E-01	2.2E+00	9.6E+00	1.30E+00	2.79E+00
5000	1.2E-01	6.4E-03	1.2E-01	7.7E-02	2.8E+00	1.2E+01	9.62E-01	2.59E+00
5200	7.9E-02	4.0E-03	7.8E-02	4.8E-02	3.5E+01	1.5E+01	7.49E-01	2.52E+00
5400	5.3E-02	2.5E-03	5.3E-02	3.1E-02	4.3E+00	1.9E+01	6.20E-01	2.53E+00
5600	3.6E-02	1.7E-03	3.6E-02	2.0E-02	5.2E+00	2.4E+01	4.85E-01	2.49E+00
5800	2.6E-02	1.1E-03	2.6E-02	1.4E-02	6.1E+00	2.9E+01	4.22E-01	2.47E+00
6000	1.8E-02	8.1E-04	1.8E-02	9.8E-03	7.2E+00	3.5E+01	3.44E-01	2.47E+00

APPENDIX C. Input Quantities Required for ALMA

ALMA solves 7 simultaneous partial differential equations for the dependent variables $u, v, \tilde{h}, k, \varepsilon, f$ and g and employs typically 21 nodes in the radial direction. The program is written in basic FORTRAN IV language and is ready to run on the CDC 6600-series computers (although only minor modifications are required to adapt it to the UNIVAC 1106/1110or IBM 360 machines). ALMA requires approximately 5 seconds compilation time on a CDC 6600 (FTN compiler) and about 40000 decimal storage locations.

Castellated profiles are assumed for the variation of the dependent variables between the grid nodes and a typical forward step size of 0.2 times the local shear layer width is employed. Approximately 5 axial steps can be executed per second.

The remainder of this appendix is concerned with the information that the user has to provide via data cards and data statements in subroutines MAIN and THERM.

Subroutine MAIN.

(i) Control indices in chapters 0 and 1:

Fortran symbol	Significance
ITDIM:	Max. number of nodes in the radial direction included in the profile plot ($\geq$N+1).

UI: Axial velocity of the inner fluid (m/s)

TI: Temperature of the inner fluid (K)

PI: Pressure of the inner fluid (N/m^2)

O2E: Mass fraction of oxygen in the outer fluid

H2OE: Mass fraction of water-vapor in the outer fluid

AN2E: Mass fraction of nitrogen in the outer fluid

TWALL: Wall temperature (K)

Subroutine THERM.

Control indices in entry BEGIN

NR: Number of reactions

NS: Number of species

HO: The quantity $\{H_{j,298.15\ K}^{-}$ $(h_{298.15\ K}-h_{o\ K})\}$ in equ.(2.2-9)

WM: Molecular weight of each species considered in the reaction.

JTDIM:	Max. number of profiles plotted at any axial location.
ILDIM:	Max. number of stations included in the longitudinal plots ($\geq$LASTEP)
JLDIM:	Max. number of longitudinal plots.
KASE:	Test case number.
NDATA:	Controls whether the input data of the equilibrium constants and enthalpy will be printed (NDATA = 1) or not (NDATA $\neq$ 1)
NSTAT:	Number of steps between output stations.
NPROF:	Number of steps between profile stations
DXPROF:	Axial distance between profile stations
NPLOT:	Number of steps between plot stations
DXPLOT:	Axial distance between plot stations
LASTEP:	Number of steps at which calculation terminates.
ISTABL:	Adjusts, if set equal to 2, the forward step DX according to local mach number.

NREACT: Controls whether the flow is chemically reacting (NREACT=2) or non reacting (NREACT=1)

MODEL: Equals 2 for turbulent flow and equals 1 for laminar flow.

(ii) Control indices and input data in chapter 2.

N: Number of grid intervals in the radial direction ($N \leq 20$)

FRA: Specifies forward step length as a fraction of the width of the shear layer.

KRAD: Specified whether the flow is axi-symmetric (KRAD=2) or plane (KRAD=1).

YOUT: Width of jet-annulus or diameter or jet-nozzle (metres)

XULAST: Maximum streamwise distance (metres).

KIN: Specifies inner boundary condition.
KIN = 1; wall boundary
KIN = 2; free boundary
KIN = 3; symmetry boundary

KEX: Specifies outer boundary condition
KEX = 1; wall boundary
KEX = 2; free boundary
KEX = 3; symmetry boundary

KONFIN: Specifies flow confinement
KONFIN = 1; confined flow
KONFIN = 2; free flow

CSALFA: Cosine of angle of inclination of streamlines to axis of symmetry

DXLIM: Controls forward step size so that entrainment per step is limited to DXLIM (fluid within boundary layer).

ULIMI: Maximum permissible dimensionless velocity difference at inner free boundary (KIN = 2).

ULIME: Maximum permissible dimensionless velocity difference at outer free boundary (KEX = 2).

(iii) Control indices in Chapter 3.

NF: Specifies the number of dependent variables to be solved for

(iv) Initial conditions in Chapter 5.

UE: Axial velocity of the outer fluid (m/s)

TE: Temperature of the outer fluid (K)

PE: Pressure of the outer fluid (N/m^2)

Data Cards.

There are 120 data cards to be read in from subroutines THERM and OUTPUT.

The first 99 cards include the values of the chemical equilibrium constants RC(60,NR) of the NR reactions and the enthalpies HT(60,NS) of the NS species. The data are read in at intervals of 100 K for temperatures up to 6000 K, so for example, HT(35,2) refers to the enthalpy at 3500 K of species 2 (oxygen).

The remaining 21 data cards contain alphanumeric data which are used to provide headings for the print-out. These are read in from OUTPUT and supply information on:

i) the dependent variables of the calculation (10 cards)

ii) the chemical reactions considered (NR cards)

iii) the species present (NS cards)

REFERENCES

1. Spalding, D. B., and B. E. Launder, "Mathematical Models of Turbulence", Academic Press, 1972.

2. Spalding, D. B., "Mathematical Models of Turbulent Flames; A Review", Imperial College Technical Report HTS/75/1, 1975.

3. Spalding, D. B., "Mathematische Modelle Turbulenter Flammen", VDI Berichte, 146, VDI Verlag, Dusseldorf, 1970.

4. Spalding, D. B., "Concentration Fluctuations in a Round Jet:, J. Chem. Eng. Sci. 26, 95, 1971.

5. Spalding, D. B., B. E. Launder, A. P. Morse and G. Maples, "Combustion of Hydrogen-air Jets in Local Chemical Equilibrium (A Guide to the CHARNAL Computer Program)", NASA CR-2407, June 1974.

6. Spalding, D. B., "A General Computer Program for Two-Dimensional Boundary Layers", Imperial College Technical Report HTS/75/17, 1975.

7. Pratap, V. S., and D. B. Spalding, "Numerical Computations of Flow in Curved Ducts", The Aeronautical Quarterly, Volume XXVI, August 1975.

8. Spalding, D. B., "The PHOENICS and CHAMPION Computer Codes", CHAM Technical Report, TR/18, 1975.